Quench-induced chaotic dynamics of Anderson-localized interacting Bose-Einstein condensates in one dimension

Swarup K. Sarkar,[1] Tapan Mishra,[2,3] Paulsamy Muruganandam,[4] and Pankaj K. Mishra[1,*]
[1]*Department of Physics, Indian Institute of Technology Guwahati, Guwahati 781039, Assam, India*
[2]*School of Physical Sciences, National Institute of Science Education and Research, Jatni 752050, Odisha, India*
[3]*Training School Complex, Homi Bhabha National Institute, Anushaktinagar, Mumbai 400094, Maharashtra, India*
[4]*Department of Physics, Bharathidasan University, Tiruchirappalli 620024, Tamilnadu, India*

(Received 21 December 2022; revised 18 May 2023; accepted 18 May 2023; published 30 May 2023)

We study the effect of atomic interaction on the localization and the associated dynamics of Bose-Einstein condensates in a one-dimensional quasiperiodic optical lattice and random disordered potentials. When the interactions are absent, the condensates exhibit localization, which weakens as we increase the interaction strength beyond a threshold value for both potential types. We inspect the localized and delocalized states by perturbing the system via quenching the interaction strength instantaneously to zero and studying the dynamics of the condensate, which we further corroborate using the out-of-time-order correlator. The temporal behavior of the time correlator displays regular dynamics for the localized state, while it shows temporal chaos for the delocalized state. We confirm this dynamical behavior by analyzing the power spectral density of the time correlator. We further identify that the condensate admits a quasiperiodic route to chaotic dynamics for both the potentials. Finally, we present the variation of the maximal Lyapunov exponents for different nonlinearity and disorder strengths that have a positive value in the regime where the time-correlator function shows chaotic behavior. Through this, we establish the strong connection between the spatially delocalized state of the condensate and its temporal chaos.

DOI: 10.1103/PhysRevA.107.053320

I. INTRODUCTION

Localization of matter waves in random media has been a topic of interest in condensed-matter physics in the past several decades [1–3]. Since the seminal prediction of the exponential localization of the electronic wave function in the presence of random disorder by Anderson (known as Anderson localization [4]), the phenomenon of localization has attracted significant attention. There have been several efforts to observe localization in various systems, such as electromagnetic waves [5–9], microwaves [10–13], and acoustic waves [14–16]. The experimental observations of matter wave localization in one-dimensional (1D) [17] and 3D [18] kicked rotors have generated significant interest in the field of ultracold matter. This field has shed light on many complex phenomena, including quantum chaos. However, in the case of noninteracting Bose-Einstein condensates (BECs) of ^{87}Rb atoms, localization was observed after releasing the condensate onto a 1D waveguide created by laser speckle [19]. Later on, Roati *et al.* discovered the localization of matter waves in BECs of ^{39}K atoms trapped in a 1D bichromatic optical lattice [20]. Further, White *et al.* reported a similar localization for the 2D noninteracting condensates of ^{87}Rb atoms trapped in a pointlike disordered potential [21]. Skipetrov *et al.* extended the analysis of the localization of condensates to 3D random potentials [22]. After the experimental observations, numerous numerical and theoretical studies were performed that show the localization of the matter wave for weak nonlinearity for the condensate trapped in the quasiperiodic potential [23–31] and random speckle potential [32–36]. There are several numerical [37] and experimental [38] works that show the destruction of localization in the presence of the interactions in the condensate and also report the subdiffusive nature of the delocalized state [37–39]. Cherroret *et al.* demonstrated theoretically that even weak interactions among particles can disrupt the transition from the subdiffusive regime to the transport inhibited regime, also known as the Anderson transition, to expand localized wave packets in 3D disordered potentials [40].

On the other hand, considerable attention has been paid to the understanding of the dynamical behavior of matter waves out of equilibrium. Several theoretical [23,27] and experimental [20,38] studies have been performed on the nonequilibrium dynamics of BECs released from an external trap in different scenarios. For instance, Doggen and Kinnunen reported the transition from the localized to the delocalized state by quenching the nonlinearity from a finite value to zero [41]. Efforts have also been made to understand the dynamics of the localized BEC trapped in disordered optical lattices. In this context, a wealth of novel scenarios has been explored both theoretically and numerically for both interacting and noninteracting condensates trapped in disordered potentials. These scenarios include enhancements in transport properties and dynamical phase transitions from superfluid to Bose glass. Kuhn *et al.* used the perturbative Green's-function

*pankaj.mishra@iitg.ac.in

 ©2023 American Physical Society

approach to show the significant role played by localization in the diffusion of noninteracting condensates trapped in a 2D speckle potential [42]. Damski *et al.* demonstrated the dynamical phase transition from a superfluid to a Bose glass for interacting condensates trapped in a 2D speckle potential [43]. Sanchez-Palencia *et al.* used theoretical and numerical calculations to show that atomic interactions in the condensate play a significant role in the dynamics for a short timescale when the condensate trapped in a 1D disordered potential is released from the trap [44]. Further, Lugan *et al.* extended this analysis to the localization of Bogolyubov quasiparticles for interacting BECs [45]. There are several works that report the presence of more complex dynamics of the condensate trapped in the random potential with the spin-orbit coupling. For instance, Mardonov *et al.* numerically demonstrated the appearance of the coexistence of two different mechanism of spin dynamics, namely, spin precession and the separation between the spin component because of anomalous spin-dependent velocities [46–48]. Interestingly, the dynamical evolution of BECs has also revealed the connection between the chaos resulting from the competing interaction and disorder in the system [49–52]. Březinová *et al.* [49] demonstrated that once BECs trapped under the harmonic potential are released from the trap and subject to either the periodic or aperiodic (quasiperiodic potential, random disordered potential, etc.) potential, the condensate shows the expansion which exhibits chaotic nature for the potential strength beyond a certain threshold value. In this work we also aim to demonstrate a similar chaotic nature of the condensate by sudden quenching of the nonlinearity of the condensate to zero.

The nonequilibrium dynamics is primarily generated in such systems by releasing the BECs from the trap [38,44] or by performing a sudden quench [53] in either coupling parameters [54,55] or nonlinear interactions [56]. Time-of-flight techniques have been quite widely used to distinguish the nature of the localized and the delocalized condensate. However, in the case of a random potential where the localization state can be more complex phases, such as the Bose glass phase and the Lifshitz phase, distinguishing the localized and the delocalized phases is more challenging and has not been done comprehensively. In this paper we use a slightly different technique to analyze the localized and delocalized states of matter waves in the presence of the quasiperiodic and the random potential. We implement the complete cessation of the nonlinear interactions of the condensate once the ground state is obtained. This process ensures the temporal dynamics in the condensate, which has been systematically captured by examining the time evolution of the time-correlator function, defined as the spatial average of the projection of the wave function at a particular instant on the stationary ground-state wave function. By making use of the time-correlator function, we observe that the localized state exhibits periodic or quasiperiodic oscillations with time and the delocalized state displays temporal chaos. We also show that the dynamical feature of the localized and delocalized states remains similar for the condensate trapped in quasiperiodic and random disordered potentials. One of the main objectives of our work is to obtain a critical value of the nonlinearity beyond which the system shows the delocalized state. For the quasiperiodic potential, the transition between the localized and the delocalized state can be ascertained on the basis of the localization length, the competition between the kinetic and interaction energies, etc. However, for the random disordered potnetial, making a distinction between these states is not so obvious because of the presence of many phases. Therefore, by studying the dynamics of the correlation function of the condensate, we provide a robust tool to establish a clear distinction between the localized and the delocalized states.

The structure of our paper is as follows. In Sec. II we provide the governing equations and numerical simulation details. It is followed in Sec. III by a brief description of different quantities, such as the time-correlation function, power spectral density (PSD), and Lyapunov exponent, which we have used to characterize the localization and chaotic dynamics of the delocalized states. In Sec. IV we present the results of the numerical simulations on the delocalization of the condensate in the quasiperiodic optical lattice and random disordered potentials. For each type of potential we analyze the effect of the increase in the nonlinear interaction on the ground state of the condensates. Further, we present the dynamics of the condensates using the time-correlator function. In Sec. V we summarize our paper.

II. NUMERICAL MODEL

We consider the condensates confined in strong transverse confinement, which can be modeled using the nondimensional 1D Gross-Pitaevskii equations (GPEs) as [23]

$$i\frac{\partial\psi(x,t)}{\partial t} = \left(-\frac{1}{2}\frac{\partial^2}{\partial x^2} + V(x) + g|\psi(x,t)|^2\right)\psi(x,t), \quad (1)$$

where $V(x)$ is the trapping potential and $g = 2a_sN/a_\perp^2$ is the nonlinearity, with a_s the s-wave scattering length, N the total number of atoms in the condensate, and $a_\perp$ the length scale corresponding to the transverse harmonic confinement [33]. We have chosen the transverse harmonic length $a_\perp = \sqrt{\hbar/m\omega_\perp}$ as the characteristic length scale (with m the mass of an atom and $\omega_\perp$ the transverse trap frequency), $\omega_\perp^{-1}$ as the characteristic timescale, and $\hbar\omega_\perp$ as the characteristic energy scale of the condensate to obtain the nondimensionalized Eq. (1). The wave function is rescaled as $\psi(x,t) = a_\perp^{1/2}\tilde{\psi}(x,t)$, where $\tilde{\psi}(x,t)$ is the nondimensionalized wave function. For brevity, we have omitted the tilde over the nondimensionalized wave function.

In this study we consider separately the trapping potential $V(x)$ as a quasiperiodic and a random disordered potential to analyze the characteristics and dynamics of the localization of the condensates. In experiments, the quasiperiodic potential can be realized as a superposition of two counterpropagating laser beams of slightly different wavelengths, which takes the form [20]

$$V(x) = \frac{4\pi^2 s_1}{\lambda_1^2}\cos^2\left(\frac{2\pi}{\lambda_1}x\right) + \frac{4\pi^2 s_2}{\lambda_2^2}\cos^2\left(\frac{2\pi}{\lambda_2}x\right), \quad (2)$$

where s_1 and s_2 denote the amplitudes of the primary and secondary lattices, respectively. Following the experimental consideration of the primary and secondary optical lattice wavelengths as $\lambda_1 = 1032$ nm and $\lambda_2 = 862$ nm [20], respectively, we take the ratio of the nondimensional wavelength (in

terms of $a_\perp \approx 1$ μm) to be $\hat{\lambda}_2/\hat{\lambda}_1 \approx 0.86$ for all our simulation runs [23].

To understand the resemblance of this localization and associated dynamical behavior to the ones in the presence of a random potential, we consider the random disordered potential consisting of N_s identical spikes randomly distributed along the x axis [57,58] in the form

$$V(x) = V_0 \sum_{j=1}^{N_s} h(x - x_j), \tag{3}$$

where V_0 is the strength of the spike and $h(x - x_j)$ is the potential of the spike at position x_j. The spike potential is considered to have the form of a Gaussian in space with width σ as [57]

$$h(x) = \frac{1}{\sigma\sqrt{\pi}} \exp\left(-\frac{x^2}{\sigma^2}\right). \tag{4}$$

The autocorrelation of $V(x)$ is defined as

$$C(d) = \langle V(x)V(x+d)\rangle - \langle V(x)\rangle^2, \tag{5}$$

where $\langle V(x)\rangle$ is the mean of the potential defined as

$$\langle V(x)\rangle \equiv \frac{1}{2L}\int_{-L}^{L} V(x)dx = \frac{V_0}{D}, \tag{6}$$

with D the average spacing between the spikes. Here the correlation length and correlation energy can be estimated by giving a fit to $C(d)$ [Eq. (5)] with a Gaussian function of the form

$$C(d) \approx V_R^2 \exp\left(-d^2/\sigma_R^2\right), \tag{7}$$

where the amplitude V_R represents the correlation energy and σ_R represents the correlation length. To generate the potential we select $N_s = 300$, $L = 30$, and width $\sigma = 0.1$. In this case, the value of the correlation energy is $V_R = 4.3974$ and $\sigma_R \approx \sqrt{2}\sigma = 0.1340$.

III. APPROACH TO CHARACTERIZING THE DYNAMICS OF THE LOCALIZED STATE

In this section we provide the details of the theoretical approach that we use to characterize the dynamics of the localized state.

A. Time-correlation function and power spectral density

For our analysis, we use the time-correlation function to characterize the dynamics of the different states. Once we obtain the ground state, we investigate the dynamics of the condensate by a sudden quenching of the nonlinearity of the condensate. The time-correlator function is defined in terms of the absolute of the overlap function as

$$c(t) = |\langle\psi(x,0)|\,\psi(x,t)\rangle|, \tag{8}$$

where $\psi(x,0)$ represents the ground state obtained using imaginary-time propagation with respect to repulsive interaction parameters. For convenience, we treat this wave function at reference time $t = 0$. After obtaining the ground state $\psi(x,0)$ we quench the nonlinearity to zero in the next time step dt and evolve the state using the GPEs (1) to obtain the evolved wave function at time t as $\psi(x,t)$ with zero nonlinearity. Here angular brackets denote the average over the entire space. The $c(t)$ can be expressed in a more explicit manner as

$$c(t) = \left|\int |\psi(x,0)|^2 \exp[-i\phi(x,t)]dx\right|, \tag{9}$$

where $\phi(x,t)$ is the phase assumed by the ground-state wave function $\psi(x,0)$ upon time evolution. The time-correlator function can be viewed as the integration of the phase acquired by the quenched state over all the spatial points at time t. There are several laboratory experiments that suggest a direct measurement of the phase acquired by the condensate using the atom interferometry [59–61]. Once the phase difference ϕ acquired by the quenched condensate is determined, the $c(t)$ can be calculated using Eq. (9).

In general, the value of the transverse frequency is $\omega_\perp = 2\pi \times 70$ Hz in a typical experiment [19]. Using this frequency strength, if we convert the real time corresponding to one time step of our simulation, which is $dt = 5 \times 10^{-4}$, we find that it comes out to be $dt \sim 1.13$ μs. Therefore, the instantaneous quenching timescale in our simulation is of the order of 1.13 μs. However, in the laboratory experiments, the quench in the nonlinear interaction is achievable through the Feshbach resonance within a typical time of about 100 μs [62,63]. We have verified our results by increasing the quenching timescale to the 100 μs considered in the experiment; however, we could not find any significant change in the results presented in this paper.

To get a deeper understanding of the dynamics and in particular the chaotic dynamics of the delocalized state, we analyze the power spectral density of the $c(t)$, which is given by [64,65]

$$\text{PSD} = \frac{1}{2\pi\mathcal{N}}|\hat{c}(\omega)|^2, \tag{10}$$

where $\hat{c}(\omega)$ is the discrete Fourier transform of the time correlator $c(t)$ evaluated at $t = mdt$ ($m = 0, 1, \ldots, \mathcal{N}$, with $\mathcal{N}$ the length of the discrete time series).

B. Lyapunov exponent

In our study, we aim to establish a possible connection between delocalization and chaos, which we execute by computing the maximal Lyapunov exponent. In dynamical systems, Lyapunov exponents are defined as the mean rate of divergence of two nearby trajectories with time. In phase space, the rate of divergence of separation between two trajectories, with an infinitesimal initial separation $\delta\boldsymbol{X}_0$, can be computed as [49]

$$|\delta\boldsymbol{X}(t)| \approx e^{\lambda t}|\delta\boldsymbol{X}_0|, \tag{11}$$

$$\lambda_{\max} = \lim_{t\to\infty}\frac{1}{t}\ln\frac{|\delta\boldsymbol{X}(t)|}{|\delta\boldsymbol{X}_0|}. \tag{12}$$

If the exponent is positive ($\lambda_{\max} > 0$), neighboring trajectories diverge exponentially, which is a signature of the chaotic behavior in the system.

In general, for the known sets of dynamical equations, the exponents can be easily computed by using the phase-space trajectory of the variables. However, computation of

the exponents directly from the time series is not so straightforward. The reconstruction of phase space from the time series data is mainly executed using the time delay τ [66] and the embedding dimension D [67]. We use the average mutual information (AMI) method to estimate the τ from the time series of the time-correlator function data, while the false nearest neighbor (FNN) method is used to compute the D [68]. The details of the AMI and FNN methods are illustrated in the Appendix. For our analysis, the usual time series of the correlator function $c(t)$ is represented in the phase space using τ and D. Further, we select a reference point on the phase-space trajectory, which is used to measure its separation from the nearest neighbor point on the phase space. We store the information of initial separation in L_0. As time progresses, the separation between the trajectory is computed until its value exceeds a threshold ϵ. Typically, we consider $\epsilon \sim O(10^{-2})$. Thereafter, the Wolf algorithm [69] is used to evaluate the Lyapunov exponents, which have three control parameters, namely, D, τ, and the threshold value of length ϵ. The Lyapunov exponent is computed using

$$\lambda_{\max} = \frac{1}{N\Delta t}\sum_{i=1}^{M-1}\log_2\frac{L_i'}{L_i}, \tag{13}$$

where N is the total number of reference points usually depending on the number of data points present in the time series, Δt is the time step associated with the time correlator, L_i and L_i' are the initial separation and the final separation measured for the ith segment of the phase-space trajectory, respectively, and M is the number of times the ratio of the final to the initial separation is calculated to complete the reference trajectory. The reference trajectory can be defined as the line from where the calculation of L_i is started by searching for the nearest neighbor point from the reference point. As time progresses, the reference point also changes on the reference trajectory to calculate the next L_i'. For our analysis we consider the embedded dimension $D = 3$ and the time step $\Delta t = 0.0005$ for a quasiperiodic potential and $\Delta t = 0.001$ for a random disordered potential.

IV. RESULTS

Here we provide detailed numerical results of the ground states and their associated dynamics. For our present analysis, we consider the quasiperiodic potential (2) and random disordered potential (3) to investigate the dynamics of the Bose gas following a quench of the initial ground state (localized or delocalized). While the imaginary-time split-step Crank-Nicolson integration scheme is used for ground-state preparation, the postquench dynamics is evolved using the real-time split-step Crank-Nicolson integration schemes [70,71]. In imaginary-time propagation, we consider $dx = 0.025$ and $dt = 0.0005$ for the simulation of the condensate trapped in a quasiperiodic potential and $dx = 0.04$ and $dt = 0.001$ for a random disordered potential. For all simulation, we use the closed boundary condition with $\psi_{\text{boundary}} = 0$. Also, we perform the grid independence test by decreasing spatial resolution to $dx = 0.007$ and find that all the results presented in the paper remain unchanged. The ground state for different nonlinearity is obtained using the imaginary-time propagation scheme in which the Gaussian wave packet centered at $x = 0$ is chosen as the initial condition.

In the following, we first present our analysis of the condensate trapped in a quasiperiodic optical lattice and then we will focus on the case of the random lattice.

A. Delocalization in the presence of the quasiperiodic optical lattice

In this section we first explore the effect of nonlinearity on the localized state of condensates trapped in the bichromatic optical lattice potential, followed by an analysis of the dynamical characteristics of the condensates once we switch off the nonlinear interactions after having the ground state of the condensate. As mentioned before, in this case, we vary λ_1 while keeping the ratio $\lambda_2/\lambda_1 \simeq 0.86$ fixed in Eq. (2). This assumption has been made by following the experimental work of Roati *et al.* [20], where the value of the transverse harmonic oscillator length was taken as $a_\perp \approx 1$ μm, which yields $\lambda_1 \simeq 1.0$ and $\lambda_2 \simeq 0.86$. In our simulations, we consider the space step as 0.025, while we fix the time step as 0.0005 [23] and use the Gaussian wave packets centered around zero as the initial conditions for all our simulations.

There are two ways in which the delocalization of the condensate trapped in the optical lattice potential can occur. One is to increase the nonlinear repulsive interaction and the other is by decreasing the disorder strength upon tuning the ratio of the laser amplitude s_2/s_1 [23,49]. We begin by analyzing the effect of nonlinearity on the localized condensates. The ground states for different localized states for weak nonlinear interaction have already been analyzed by Adhikari and Salasnich [23]. As we are interested in the analysis of the dynamics of these states, to make the paper self-contained, in the following we briefly present the nature of different ground states for various nonlinearities.

In Fig. 1(a) we show the spatial distribution of the ground-state density for different nonlinear interactions with $s_1 = 3.0$, $s_2/s_1 = 1.0$, and $\lambda_1 = 10$. It is easy to see that for the noninteracting case ($g = 0$), the condensate gets localized within $-5 \lesssim x \lesssim 5$ with the maximum density around $x \sim \pm 2$. As we increase the nonlinearity to $g = 2$, we notice a decrease in the density around the central region ($x \sim 0$), resulting in the appearance of peaks at larger values of x. However, the condensate appears to be confined within $-10 \lesssim x \lesssim 10$. Further, an increase in the nonlinearity to $g = 4$ results in an expansion of the localized condensate in the space. As the nonlinearity exceeds a threshold value ($g \gtrsim 5$), the matter wave localization gets destroyed, which is quite noticeable from the nature of the condensate that appears to span the whole box as shown for $g = 8$ (pink line) and $g = 10$ (brown line) in Fig. 1(a). These features are more noticeable from the behavior of the tail of the density profile that displays an exponential fall in the localized state, a feature which is absent for the delocalized state [cf. Fig. 1(b)].

For comparison, we also undertake a similar analysis of the localization by lowering the strength of the quasiperiodic optical lattice to $s_2/s_1 = 0.5$. Figure 2 illustrates the spatial profile of the ground state of the matter wave density for different nonlinearities. We find that, in this case also, the matter wave remains localized for low nonlinearity, as expected. As we increase the nonlinearity, the condensate gets delocalized

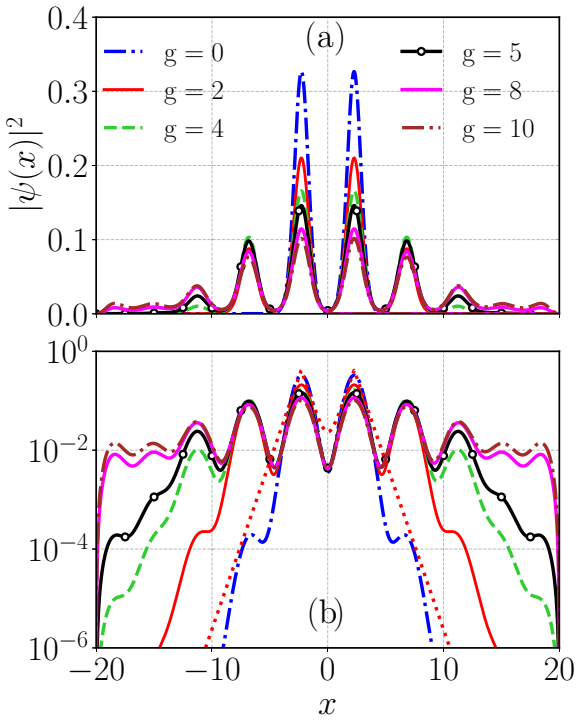

FIG. 1. Variation of density with different nonlinearity for $\lambda_1 = 10$, $\lambda_2/\lambda_1 = 0.86$, $s_1 = 3$, and $s_2/s_1 = 1.0$ in the (a) linear and (b) semilogarithmic scale. The wave function gets localized near $x = 0$ for $g = 0$. Increasing the nonlinearity results in the spread of the wave function. In the localized states ($g = 0, 2, 4$), the condensate density exhibits an exponential tail. For $g \gtrsim 5$, the condensate spans the whole box, exhibiting delocalized nature. In (b) the red dotted line represents the double exponential fit to the condensate ground state for $g = 0$.

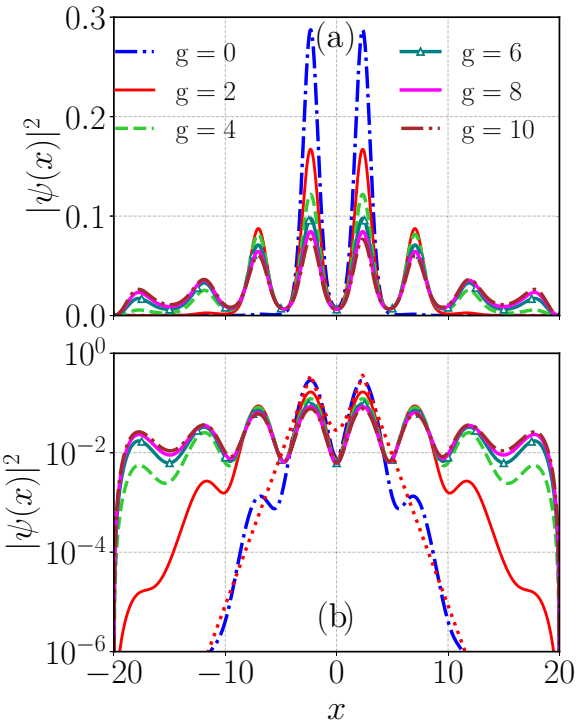

FIG. 2. (a) Spatial profile of the condensate density for different nonlinearities at $s_2/s_1 = 0.5$. The other parameters are the same as those in Fig. 1. The condensate exhibits localized nature for noninteracting cases ($g = 0$), which further shows delocalization upon increasing the nonlinearity ($g \gtrsim 4$). (b) Density variation in semilogarithmic scale for different nonlinearities. The red dotted line represents the double exponential fit to the condensate ground state for $g = 0$. The exponential fall of the condensate density around its center characterizes the localization behavior. The density exhibits delocalized states with increasing nonlinearities.

at a smaller g ($\gtrsim$4) than those for higher disorder strength ($s_2/s_1 = 1.0$), which happens at $g \gtrsim 5$.

To quantify this transition from the localized to the delocalized state, we compute the localization length by fitting the localized states with the function $y = ae^{-|x-x_0|/L_{\rm loc}} + ae^{-|x+x_0|/L_{\rm loc}}$, where $L_{\rm loc}$ is the localization length, a is the parameter, and x_0 is the localization center. The variation of $L_{\rm loc}$ with respect to g is plotted in Fig. 3 for different values of s_2/s_1. We find that when the condensate is in the localized state, the $L_{\rm loc}$ varies linearly with g. However, a discontinuous jump occurs in $L_{\rm loc}$ for a certain value of g, beyond which the delocalization happens in the density profile. The threshold value of the nonlinearity at which the delocalization occurs decreases when we decrease the disorder strength s_2/s_1.

To elucidate the transition of the condensate from the localized to the delocalized state, it is pertinent to include the relevant physical cause. To achieve this, we compute the energies of different components, such as the kinetic energy $E_k = \frac{1}{2}\int dx|\nabla\psi|^2$, potential energy $E_{\rm pot} = \int V(x)|\psi|^2 dx$, and interaction energy $E_{\rm int} = \frac{1}{2}\int g|\psi|^4 dx$, where ψ is the ground-state wave function obtained by using imaginary-time propagation of Eq. (1) with finite g. In Fig. 4 we present the variation of different energies E_k (■), $E_{\rm int}$ (●), and $E_{\rm pot}$ (⬢) for different s_2/s_1. We observe that while $E_{\rm pot}$ and $E_{\rm int}$ increase, E_k decreases with an increase in g. Interestingly, we find that below the threshold value of the critical nonlinear strength g_c, E_k dominates over $E_{\rm int}$, while we observe the opposite trend

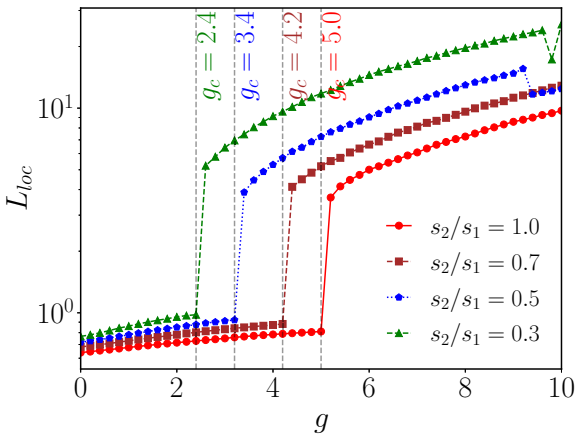

FIG. 3. Variation of localization length $L_{\rm loc}$ with the nonlinearity for different s_2/s_1. The $L_{\rm loc}$ is calculated using the $1/e$ fall of the fitted curve $ae^{-|x-x_0|/L_{\rm loc}} + ae^{-|x+x_0|/L_{\rm loc}}$, with x_0 the point of maximum density in space. Here $x_0 = \pm 2.275$. The $L_{\rm loc}$ starts increasing beyond g_c. The g_c increases upon an increase in s_2/s_1. The other parameters are the same as those in Fig. 1.

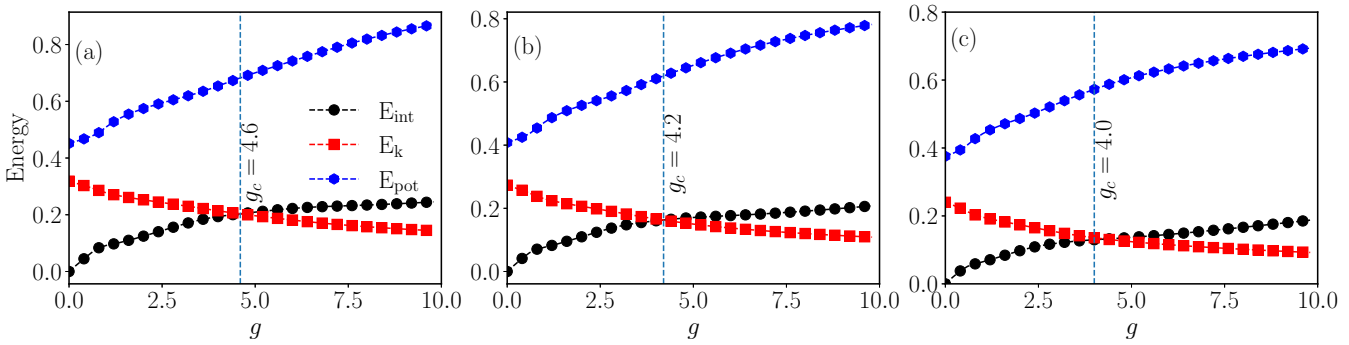

FIG. 4. Variation of interaction E_{int} (●), kinetic E_k (■), and potential E_{pot} (⬢) energies with nonlinear interaction for different disorder strengths (a) $s_2/s_1 = 1.0$, (b) $s_2/s_1 = 0.7$, and (c) $s_2/s_1 = 0.5$. All the other parameters are the same as in Fig. 1. In the localized regime E_k dominates over E_{int}; however, in the delocalized regime E_{int} dominates over E_k. The threshold nonlinear interaction g_c for different s_2/s_1 values is consistent with that obtained from the localization length. The vertical lines are drawn to guide the eyes for g_c.

above the critical g_c. This trend holds for all values of s_2/s_1 considered.

In the following, we will analyze the characteristics of these states using their dynamical evolution.

Quench dynamics of the localized and delocalized states

To study the detailed dynamics of the localized and delocalized condensates, we consider the ground states obtained for different nonlinearity and perform the time evolution by applying an instantaneous quench of the nonlinear interaction to zero. This protocol introduces the dynamics in the condensates, which have been captured by evolving the GPEs using the real-time scheme [70].

To probe the spatiotemporal evolution after quenching of the condensate prepared at different values of g, in Fig. 5 we plot the spatiotemporal evolution of the density of the condensates after sudden cessation of g. For $g = 0$, the localized condensate propagates with time without any distortion, as can be seen in Fig. 5(a). However, the localized condensate at $g = 4$ develops oscillatory behavior, as depicted in Fig. 5(b). The oscillatory behavior becomes more and more irregular for higher values of nonlinearity [cf. Figs. 5(c) and 5(d)]. Interestingly, we find that the condensate, which was in the delocalized state, exhibits chaotic oscillation with time, as depicted in Fig. 5(d) (for $g = 10$). Note that the absence of any spatial change in the condensate after the quench may be attributed to the fact that the condensate is trapped tightly near the minimum of the external potential and it remains so with zero nonlinear interaction as time progresses. Also, the dispersion due to the kinetic part is quite low because the trapped energy dominates over other energies for all values

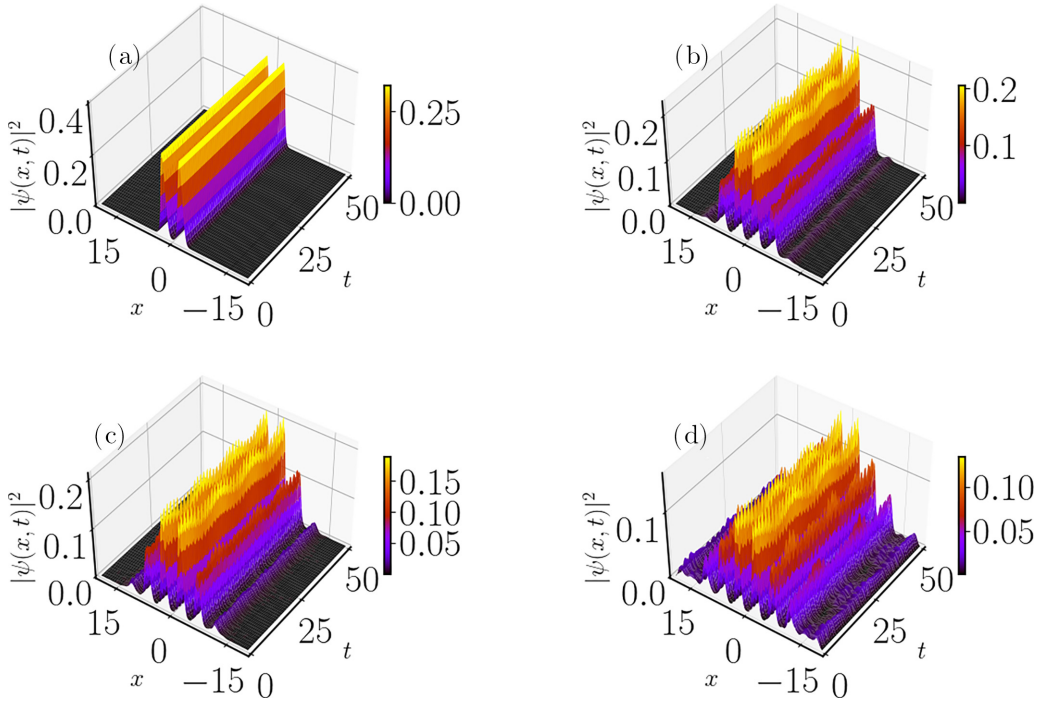

FIG. 5. Pseudocolor representation of the spatiotemporal evolution of the condensate after quenching the nonlinearity to zero as the ground state is prepared for different g: (a) $g = 0$, (b) $g = 4$, (c) $g = 5$, and (d) $g = 10$. The other parameters are the same as in Fig. 1.

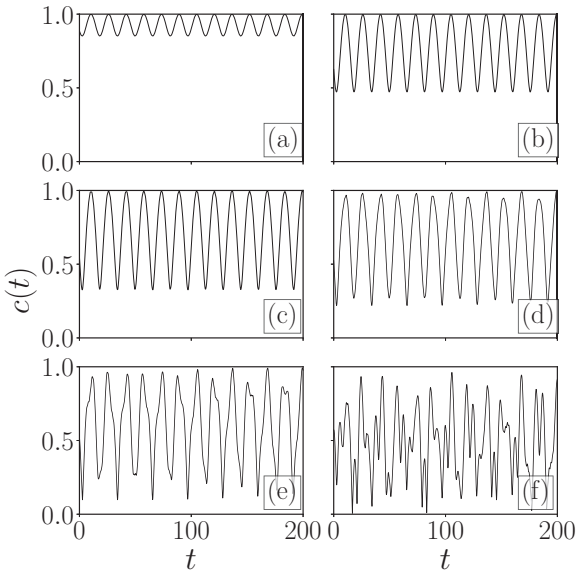

FIG. 6. Temporal variation of the time-correlation function $c(t)$ at $s_2/s_1 = 1.0$, $s_1 = 3$, and $\lambda_1 = 10.0$ for different nonlinearities (a) $g = 1$, (b) $g = 2$, (c) $g = 3$, (d) $g = 4$, (e) $g = 5$, and (f) $g = 10$. In the localized state ($g \lesssim 5$), $c(t)$ exhibits periodic or quasiperiodic behavior, which becomes chaotic in the delocalized state. The time period corresponding to periodic oscillation is $T \approx 15.426$ (i.e., $\omega \approx 0.407$).

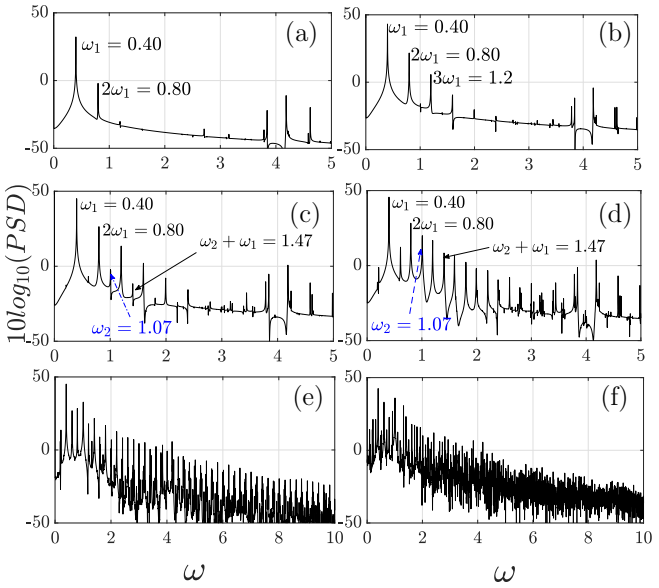

FIG. 7. PSD of the time-correlation function (Fig. 2) for different nonlinearities (a) $g = 1$ (periodic), (b) $g = 2$ (periodic), (c) $g = 3$ (quasiperiodic), (d) $g = 4$ (quasiperiodic), (e) $g = 5$ (chaotic), and (f) $g = 10$ (chaotic). The other parameters are the same as in Fig. 2. An increase in the nonlinearity leads to the generation of two incommensurate frequencies $\omega_1 = 0.40$ and $\omega_2 = 1.07$ at $g \sim 3$. Finally, a large number of frequencies get generated, a signature of chaotic behavior at higher nonlinearity ($g \gtrsim 5$).

of s_2/s_1 (see Fig. 4). The role of the random potential here is to contribute to the spatial phase with a random value in the condensate with the time, which also reflects in the temporal behavior of the time-correlator function, which we will discuss later.

We investigate the dynamics of the localized matter wave density by computing the time correlator $c(t)$ [Eq. (8)] and analyzing its temporal evolution. For this, we consider the ground state obtained for a particular g as $\psi(0)$ and the condensate wave function at a time t after quenching of the finite nonlinearity to zero as $\psi(t)$. In Fig. 6 we show the temporal evolution of $c(t)$ for the ground state prepared at different values of g. Figures 6(a)–6(f) depict the evolution of $c(t)$ for $g = 1$, 2, 3, 4, 5, and 10, respectively. For the localized state prepared at $g = 1$, $c(t)$ exhibits periodic oscillations of amplitude very close to unity. The localized state with $g = 2$ shows similar oscillatory behavior, as shown in Fig. 6(b). For $g = 3$, $c(t)$ displays some modulated oscillation, indicating the presence of more than one frequency. However, for $g = 5$ and 10, which correspond to a delocalized condensate, $c(t)$ exhibits aperiodic or chaotic temporal features. This indicates that quenching of nonlinearity generates periodic, quasiperiodic, and chaotic dynamics depending on whether the corresponding ground state is localized or delocalized.

To further investigate the nature of the different frequencies present in the dynamics and the route to chaotic behavior of the delocalized state, we compute the PSD of the time correlator, using the formula defined in Eq. (10), corresponding to the periodic, quasiperiodic, and chaotic states as discussed above. Figure 7 depicts the PSD of $c(t)$ corresponding to the periodic, quasiperiodic, and chaotic states. We see that the periodic behavior of the dynamical state for $g = 1$ involves the fundamental frequency $\omega_1 = 0.40$ together with the presence of its higher harmonics [see Fig. 7(a)]. We observe similar behavior in the dynamics of the localized state at $g = 2$, as depicted in Fig. 7(b). The PSD of $c(t)$ for $g = 3$ shows peaks at the frequencies at $\omega_1 = 0.40$ and $\omega_2 = 1.07$ [see Fig. 7(c)]. The irrational ratio of the two frequencies indicates the quasiperiodic nature of $c(t)$ for $g = 3$. Further, for $g = 4$ [Fig. 7(d)], apart from the frequencies ω_1 and ω_2, other higher frequencies around ω_1 and ω_2 as well as subharmonics, such as $\omega_2 + \omega_1$, $\omega_2 + 2\omega_1$, etc., start appearing. We notice that more frequencies start getting populated around ω_1 and ω_2 for the dynamics of the condensate that show a delocalized state for higher nonlinearity (for $g \gtrsim 4$) as depicted in Figs. 7(e) and 7(f). The exponential fall behaviour of PSD with the frequencies in the dynamics of the delocalized state confirms the fully developed temporal chaos [72,73]. The inverse of the rate of decay ($\tilde{\mu}$) of the PSD with the frequency of the chaotic state is of the order of approximately 1.4 in the high-frequency range. In general, $\tilde{\mu}$ is related to the Lyapunov exponent [72]. We find that the dynamics of the localized state exhibits periodic oscillations for a weak nonlinear interaction, which transforms into quasiperiodic for a stronger nonlinear interaction. The value of g at which the condensate exhibits delocalized nature has a chaotic time correlator. With this, we find a systematic generation of the frequencies that finally leads to the chaotic dynamics of the delocalized state, which suggests a quasiperiodic route to chaos. We find the presence of the same quasiperiodic route to chaos for the lower disorder strengths (s_2/s_1), which we discuss below.

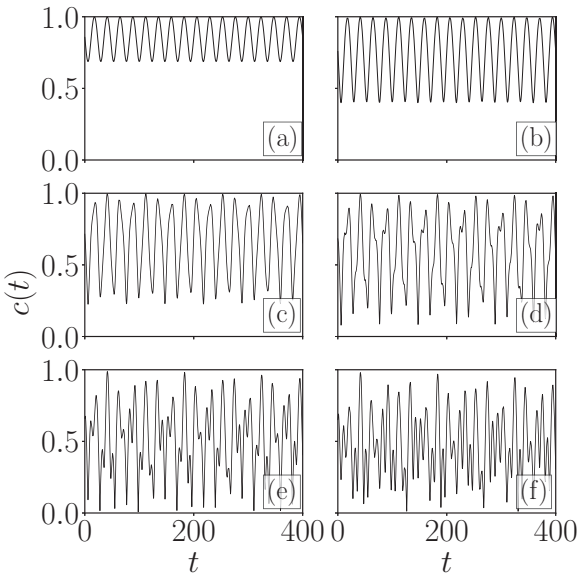

FIG. 8. Temporal evolution of the time-correlator function at $s_2/s_1 = 0.5$, $s_1 = 3$, and $\lambda_1 = 10.0$ for different nonlinearities (a) $g = 1$, (b) $g = 2$, (c) $g = 3$, (d) $g = 4$, (e) $g = 5$, and (f) $g = 10$. The temporal behavior of the localization and delocalization behavior have qualitative features similar to those for $s_2/s_1 = 1.0$; the only difference is reflected in the decrease in the nonlinearity, at which the correlation shows the chaotic behavior. The time period for the periodic oscillation is $T \approx 23.691$ ($\omega \approx 0.265$).

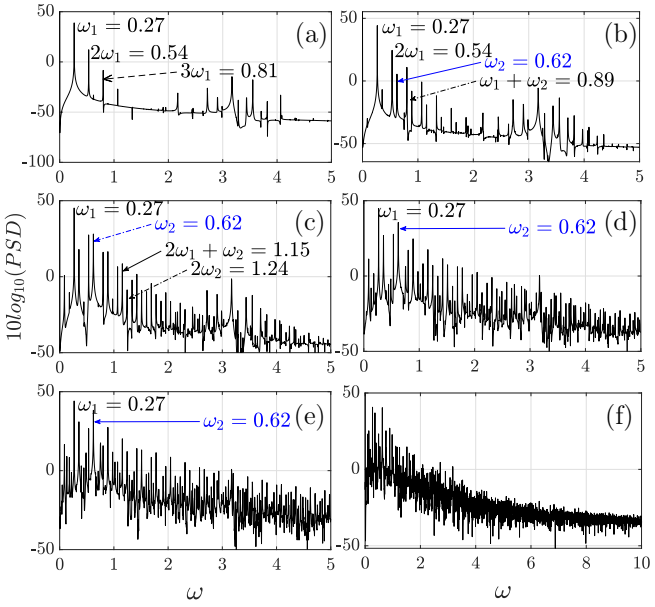

FIG. 9. PSD of time-correlator function shown in Fig. 8 at different nonlinearities (a) $g = 1$, (b) $g = 2$, (c) $g = 3$, (d) $g = 4$, (e) $g = 5$, and (f) $g = 10$. The other parameters are the same as in Fig. 7. The system undergoes a transition from the localized ($g = 1, 2, 3$) to the delocalized state ($g = 4, 5, 10$) with the appearance of frequencies around quasiperiodic frequencies ω_1 and ω_2 in the PSD of the time-correlation function upon increasing the nonlinearity.

We now focus on investigating the nature of the dynamics of the condensate for a lower disorder strength ($s_2/s_1 = 0.5$). In Fig. 8 we plot $c(t)$ for different values of g. Here the amplitude of $c(t)$ appears to be slightly higher than those obtained for $s_2/s_1 = 1$ (Fig. 6) after quenching the nonlinearity (from $g = 1$ to $g = 0$). Similar to the higher disorder strength, in the case of $s_2/s_1 = 0.5$, $c(t)$ shows periodic [Figs. 8(a) and 8(b)], quasiperiodic [Figs. 8(c) and 8(d)], and chaotic oscillations [Figs. 8(e) and 8(f)] as the nonlinearity is quenched from $g = \{1, 2\}$, $\{3, 4\}$, and $\{5, 10\}$ to zero, respectively. One noticeable effect of the disorder strength s_2/s_1 is observed in terms of the magnitude of the fundamental (ω_1) and quasiperiodic frequencies (ω_1 and ω_2), which decrease with the decrease in s_2/s_1.

In Fig. 9 we illustrate the PSD of the time correlator presented in Fig. 8. Figure 9(a) shows the presence of fundamental frequency $\omega_1 = 0.27$ along with its higher harmonics $2\omega_1 = 0.54$ and $3\omega_1 = 0.81$ in the dynamics of the localized state when the nonlinearity is instantaneously quenched from $g = 1$ to $g = 0$. In the case of the quench dynamics of the high nonlinearity state, for example, $g = 2$, we find other eigenfrequencies such as $\omega_2 = 0.62$, apart from the fundamental frequency at $\omega_1 = 0.27$, which indicates the quasiperiodic nature of $c(t)$. At higher nonlinearity $g \gtrsim 4$, more frequencies around ω_1 and ω_2 start getting populated [see Figs. 9(d)–9(f)]. The appearance of other frequencies in the case of the delocalized state (for quenching from $g = 4$ to $g = 0$) the PSD exhibits exponential decay behavior, indicating the presence of chaotic dynamics. We find that for $s_2/s_1 = 0.5$, the chaotic dynamics appears for the state when $g \gtrsim 4$, which is lower than that for $s_2/s_1 = 1$. However, it is interesting to note that for both disorder strengths ($s_2/s_1 = 0.5, 1$), a quasiperiodic route to chaos is observed in the dynamics when the condensate makes a transition from the localized to the delocalized state.

To further quantify the chaotic nature of the dynamics in a more systematic manner, we compute the maximal Lyapunov exponent $\lambda_{\max}$ as given in Eq. (12) corresponding to the dynamics of the condensate using the time series of the time-correlator function $c(t)$. In Fig. 10 we show the variation of $\lambda_{\max}$ with the interaction strength for different values of s_2/s_1. The increase of $\lambda_{\max}$ towards the positive value indicates the chaotic nature of the time-correlator function. We find that the Lyapunov exponent fluctuates about zero until $g \sim 4.8$ for $s_2/s_1 = 1$. When $g \gtrsim 4.8$, we witness a systematic increase in the Lyapunov exponent and remains positive ($\lambda_{\max} > 0$), indicating the chaotic nature of the time-correlator functions for that range of g. Therefore, the above analysis provides the value of the critical nonlinearity, beyond which the condensate has a delocalized state and thus the corresponding dynamics is chaotic. Lowering the disorder strength results in a decrease in the value of the critical nonlinearity g_c beyond which $\lambda_{\max}$ becomes positive. Further, for $s_2/s_1 = 0.5$, the critical nonlinearity beyond which the condensate has chaotic dynamics is $g_c \sim 4$, while for $s_2/s_1 = 0.3$ it is $g_c \sim 2.4$. Note that the value of g_c calculated through this analysis provides accurate nonlinearity at which the condensate is delocalized in space and has dynamically chaotic behavior, which may be important feedback for the experiments. At this juncture, it is worth mentioning that Březinová *et al.* [49] observed a similar kind of chaotic behavior in the dynamics of the delocalized state when the condensate was subject to a weak periodic trap or

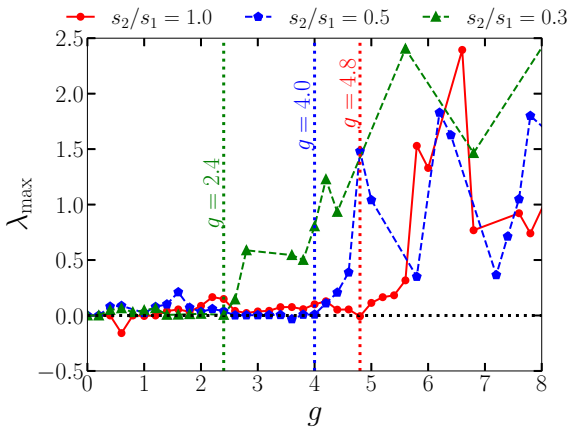

FIG. 10. Variation of the Lyapunov exponent $\lambda_{\max}$ against nonlinearity for different disordered strengths $s_2/s_1 = 1$ (solid line with red circles), $s_2/s_1 = 0.5$ (dashed line with blue pentagons), and $s_2/s_1 = 0.3$ (dashed line with green triangles). For the localized state $\lambda_{\max} \lesssim 0$, while for the delocalized state $\lambda_{\max} > 0$, indicating the chaotic dynamics. The threshold g_c above which $\lambda_{\max} > 0$ (a characteristic of the delocalized state) decreases upon the decrease in s_2/s_1. Vertical dotted lines are drawn to guide the eyes for different g_c.

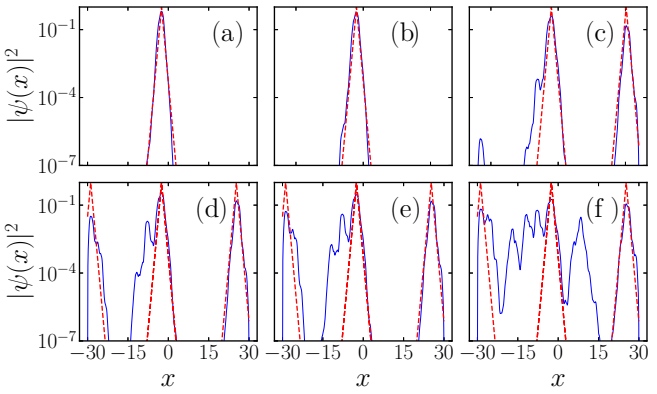

FIG. 11. Variation of density (in semilogarithmic scale) at $V_0 = 1.0$ for different nonlinearities (a) $g = 0$, (b) $g = 1$, (c) $g = 3$, (d) $g = 4$, (e) $g = 5$, and (f) $g = 10$. The red dashed line is the exponential function drawn near the localized region to guide the eyes to show the deviation of the matter wave from the localized nature.

an aperiodic (quasiperiodic and random disordered potential) trap.

So far, we have analyzed the dynamics of the condensates in the presence of the quasiperiodic potential and found that while the localized state exhibits either periodic or quasiperiodic dynamics, delocalized states show chaotic dynamics upon quenching the nonlinearity to zero. Also, the route to chaos upon increasing the nonlinear interaction appears to be quasiperiodic in nature. Several studies indicate the similarity in the condensate dynamics for the condensate trapped in the quasiperiodic potential and in the random-speckle potential [49]. To further clarify this interesting feature, in the following section we present the spatial and temporal behaviors of the condensate in the presence of the random disordered potential.

B. Delocalization in the presence of the random disordered potential

In this section we discuss the effect of the nonlinearity on the localized condensate trapped in the random disordered potential. The details to generate the random potential are given in Sec. II. First, we discuss the ground state of the condensate trapped in the random disordered potential at different nonlinearities for single disorder realization. Then we discuss the dynamics of the condensate along a similar line of analysis performed for the condensate trapped in a quasiperiodic potential, where we use the quenching of a nonlinear interaction from a finite value to zero to generate the dynamics. Finally, we characterize the dynamics using the PSD and largest Lyapunov exponent analysis of the time-correlator function.

Apart from the localized and delocalized states such as those observed for a quasiperiodic potential, we also witness the presence of a Bose glass phase for the condensate trapped in the random disordered potential [74–77]. Lugan *et al.* demonstrated theoretically that the condensate undergoes a transition from a Lifshitz glass to a delocalized state upon the increase of the nonlinear interaction [78]. In Fig. 11 we plot the density profile (blue solid line) in a semilogarithmic scale for different values of g. Here the red dashed lines are the exponential curve near the localized region drawn to display an estimate of the exponential fall of the density in space. For the noninteracting condensate, i.e., $g = 0$, the density profile shows the exponential fall, which is quite evident from the excellent matching of the density profile with the drawn exponential curve [see Fig. 11(a)] complementing the localized nature of the condensate. The spatial profile of the condensate for $g = 1$ also shows an exponential fall as depicted in Fig. 11(b). However, as discussed earlier, due to the random nature of the potential, we witness the presence of another region of the localized condensate, apart from what is present near $x \sim 0$, on increasing g further. For instance, at $g = 3$, one part of the condensate gets localized near $x = 0$, while another part gets localized near $x \sim 25$. The condensate near both regions appears to fall exponentially, which is quite clear from the fitting of the spatial profile of the condensate with the exponential curve (red dotted line). Note that such a bifurcation of the condensate into multiple localized states is in general termed fragmented BECs [33,79] or Bose glass [75–77]. However, a further increase in g ($\gtrsim 5$) results in the deviation of the tail of the localized condensate from the exponential nature, as apparent from Figs. 11(d)–11(f), also termed the delocalized state.

Next we will characterize the different ground-state phases of the condensate trapped in the random potential, namely, the localized state (LS) for a weak interaction, Bose glass (BG) for an intermediate interaction, and delocalized Bose-Einstein condensate (DBEC) for large nonlinear interaction. We will do so using the chemical potential μ defined as

$$\mu = \int dx \left[\frac{1}{2} |\nabla \psi|^2 + V(x)|\psi|^2 + g|\psi|^4 \right], \qquad (14)$$

where ψ corresponds to the ground-state wave function. In Fig. 12(a) we plot μ as a function of g for three different random realizations (R_1, R_2, and R_3). For all realizations, μ shows a sharp increase with g. The rate of increase of μ with

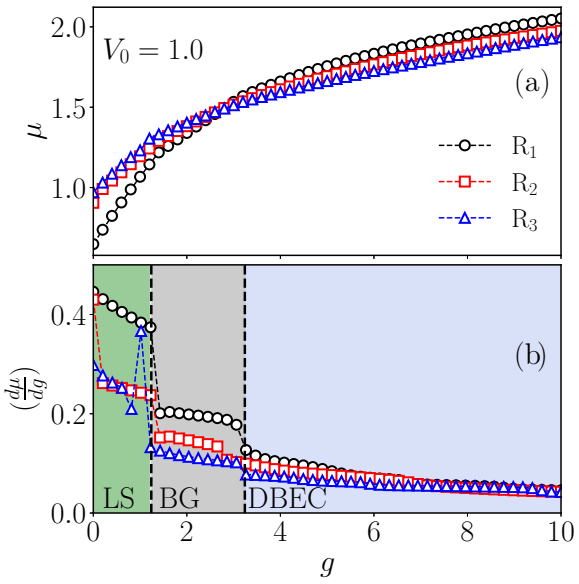

FIG. 12. Different states of the condensate trapped in the random disordered potnetial of strength $V_0 = 1.0$ based on the nature of μ in different ranges of g. The other parameters are the same as Fig. 11. (a) Variation of chemical potential μ with g for three different random realizations R_1 (black circles), R_2 (red squares), and R_3 (blue triangles). (b) Variation of $d\mu/dg$ with g distinguishing different regimes for the condensate: the localized state for lower g with higher $d\mu/dg \sim 0.2$–0.4, the Bose glass state at intermediate g with $d\mu/dg \sim 0.12$–0.2, and the delocalized BEC state at higher g with $d\mu/dg \sim 0.05$–0.12. The vertical dotted lines are drawn to guide the eyes to distinguish different localized states of the condensate.

g keeps decreasing with the increase in g. In order to quantify the distinct nature of the variation of μ, we compute $d\mu/dg$ for different g. As the compressibility of the condensate is $\kappa \propto (d\mu/dn)^{-1}$, where n is the condensate density which is a function of g, the inverse of $d\mu/dg$ can also be attributed to the compressibility of the gas. In Fig. 12(b) we display $d\mu/dg$ for different g for all the realizations (R_1, R_2, and R_3) presented in Fig. 12(a). In the LS, $d\mu/dg \sim 0.2$–0.4 has the largest value, the intermediate value of $d\mu/dg \sim 0.12$–0.2 represents the BG state, and the lowest $d\mu/dg \sim 0.05$–0.12 represents the DBEC state. Overall, we find that the compressibility is higher for the DBEC phase, intermediate for the BG, and smallest for the LS, which is in accordance with the typical behavior of localized and delocalized gases. The trend observed for μ in different regimes of the condensate trapped in the random potential is consistent with earlier studies [75–77]. In Fig. 13 we show the density profile in the semilogarithmic scale for $V_0 = 0.5$ of the random disordered potential. For this parameter, we find that for the lower nonlinearity ($g \lesssim 3$) the condensate is localized and we observe a delocalized state for higher nonlinearities. However, all the phases, like the LS, BG, and DBEC, are of similar nature to those for $V_0 = 1$ (see Fig. 11). It is straightforward to see that decreasing the potential strength decreases the critical nonlinearity above which the condensate gets delocalized, which is around $g_c \sim 3$ for $V_0 = 0.5$ compared to $g \sim 5$ for $V_0 = 1$. To further identify the different regions of the condensate upon increasing the

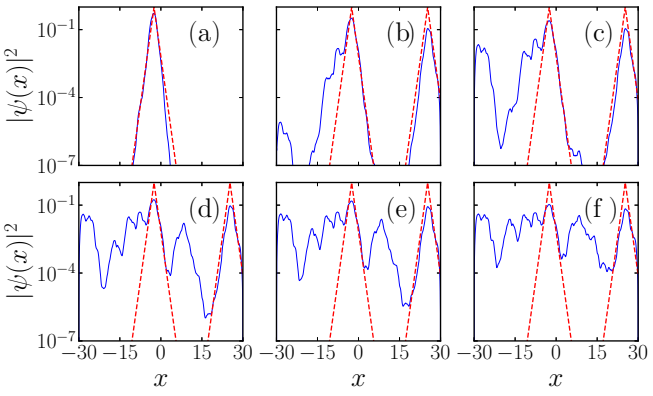

FIG. 13. Variation of density (in semilogarithmic scale) trapped in the random potential at $V_0 = 0.5$ with different nonlinearities (a) $g = 0$, (b) $g = 2$, (c) $g = 3$, (d) $g = 5$, (e) $g = 6$, and (f) $g = 10$. The red dashed line is the exponential function drawn near the localized region to guide the eyes to show the deviation of the matter wave from the localized nature.

nonlinearity, in Fig. 14 we show the variation of μ and $d\mu/dg$ with g for $V_0 = 0.5$ in Figs. 14(a) and 14(b), respectively. For this case also we obtain the presence of different regimes based on the values of $d\mu/dg$ from those observed for $V_0 = 1.0$. Note that although μ is lower for $V_0 = 0.5$ than for $V_0 = 1$, the value of $d\mu/dg$ for different regimes of localization appears to be the same.

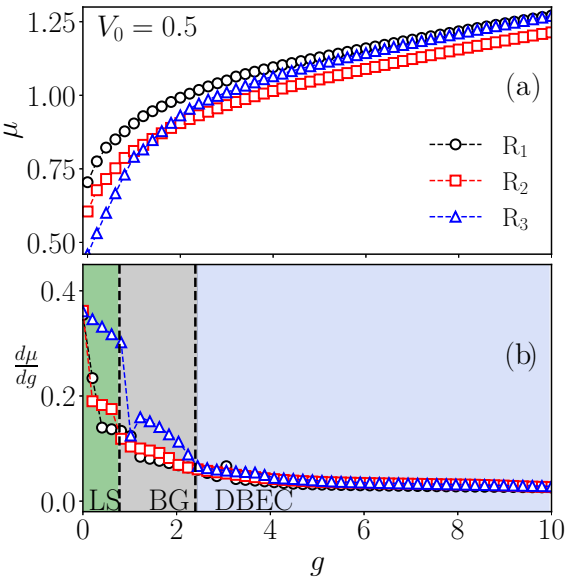

FIG. 14. Different states of the condensate trapped in the random disordered potnetial of strength $V_0 = 0.5$ based on the nature of μ in different ranges of g. The other parameters are the same as in Fig. 13. (a) Variation of chemical potential μ with nonlinear interaction g for three different random realizations R_1 (black circles), R_2 (red squares), and R_3 (blue triangles). (b) Variation of $d\mu/dg$ with g distinguishing different regimes for the condensate: the localized state for lower g with higher $d\mu/dg \sim 0.12$–0.36, the Bose glass state at intermediate g with $d\mu/dg \sim 0.06$–0.12, and the delocalized BEC state at higher g with $d\mu/dg \sim 0.04$–0.06. The vertical dotted lines are drawn to guide the eyes to distinguish different localized states of the condensate.

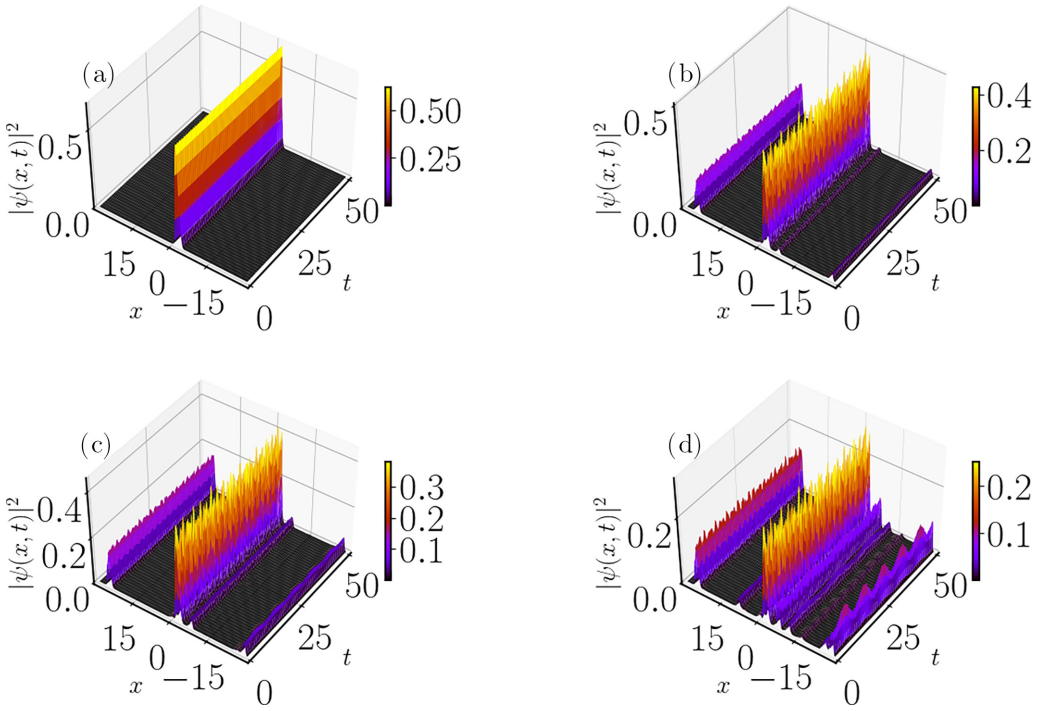

FIG. 15. Spatiotemporal evolution of the condensate at different nonlinearities (a) $g = 0$, (b) $g = 4$, (c) $g = 5$, and (d) $g = 10$ trapped under the Gaussian random disordered potential for $V_0 = 1.0$. The condensate remains localized near $x = -2.51$ for low nonlinearity $g = 1$. An increase in the nonlinearity results in the delocalized condensate along with more fluctuations in the density, especially near $x = 0$.

In the following, we present the dynamics of the different states observed for the condensate trapped in the random disordered potential.

Quench dynamics of the condensates trapped in the random potential

In Fig. 15 we depict the spatiotemporal evolution of the condensate density after quenching of the nonlinearity to zero from different initial values of g. For $g = 0$ [cf. Fig. 15(a)], the localized condensate propagates with time without any distortion. The condensate develops fluctuation with time upon the increase in the value of g [see Figs. 15(b)–15(d)], especially near the region $x = 0$. The temporal oscillation becomes more irregular for higher nonlinearity, and the corresponding dynamics display chaos, a dynamical feature similar to that obtained for the condensate trapped in the quasiperiodic potential. Note that, as discussed for the situation of no expansion in the x direction for the condensate trapped in a quasiperiodic potential, once the dynamics appears due to quenching in the nonlinearity, we find a similar scenario for the condensate dynamics trapped with a random potential. In this case, we also observe that the potential energy dominates over the kinetic and thus does not allow the condensate to diffuse around the minimum of the potential well.

We characterize the condensate dynamics by analyzing the temporal evolution of $c(t)$ for different values of g, which are plotted in Fig. 16. Figure 16(a) illustrates the periodic temporal evolution of $c(t)$ with a period $T \approx 1.309$ for the localized state upon quenching the nonlinearity from $g = 1.6$ to $g = 0$. Figure 16(b) shows the evolution of $c(t)$ for the localized state when g is quenched from $g = 2$ to $g = 0$. The corresponding dynamics shows the quasiperiodic oscillation with the presence of two frequencies, which becomes more pronounced for $g = 3$, as depicted in Fig. 16(c). As we analyze the quench dynamics for the state at higher nonlinearity

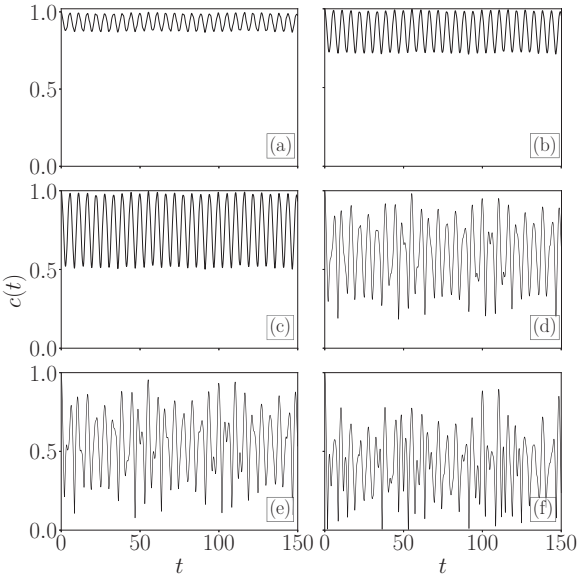

FIG. 16. Temporal evolution of the time-correlation function for quenching from (a) $g = 1.6$, (b) $g = 2$, (c) $g = 3$, (d) $g = 5$, (e) $g = 6$, and (f) $g = 10$ to $g = 0$. The other parameters are the same as in Fig. 11. In the localized state ($g \lesssim 5$), the correlation function exhibits a periodic or quasiperiodic oscillation, which becomes chaotic at higher g. Here the disorder strength $V_0 = 1.0$.

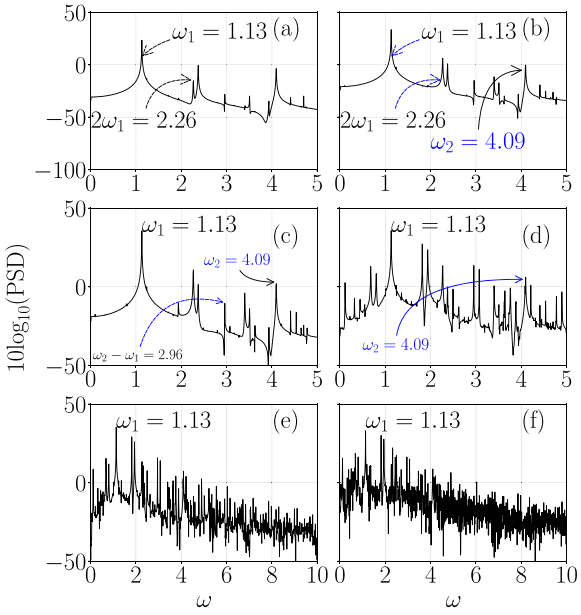

FIG. 17. PSD of time-correlation function (as shown in Fig. 16) for the situation when the nonlinearity is quenched from (a) $g = 1.6$, (b) $g = 2$, (c) $g = 3$, (d) $g = 5$, (e) $g = 6$, and (f) $g = 10$ to $g = 0$ for $V_0 = 1.0$. Increasing the nonlinearity generates two incommensurate frequencies $\omega_1 = 1.13$ and $\omega_2 = 4.09$ at $g \sim 2$. Finally, the region near these frequencies starts getting populated, leading to the chaotic behavior at higher nonlinearity ($g \gtrsim 5$).

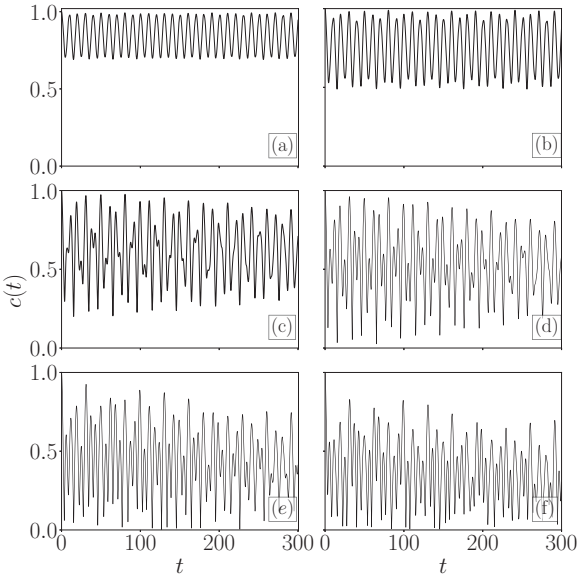

FIG. 18. Variation of the time-correlation function with time at $V_0 = 0.5$ after quenching the steady state from (a) $g = 1.4$, (b) $g = 2.0$, (c) $g = 3$, (d) $g = 4$, (e) $g = 6$, and (f) $g = 10$ to $g = 0$. The other parameters are the same as in Fig. 13. In the localized state ($g \lesssim 4$), the correlation function exhibits either a periodic ($g = 1.4$) or quasiperiodic ($g = 1.6, 2, 3$) oscillation, which becomes chaotic after quenching the system from higher nonlinearity.

($g \gtrsim 5$) for which the ground state exhibits a delocalized nature, we find that the corresponding $c(t)$ exhibits aperiodic or chaotic oscillation [see Figs. 16(d)–16(f)]. These dynamical behaviors for different states will become clear as we investigate the PSD of the time correlation, which we discuss below. In Fig. 17 we plot the PSD of the time-correlation function presented in Fig. 16. The PSD for the localized state quenched from $g = 1.6$ to $g = 0$ is illustrated in Fig. 17(a). It shows the presence of fundamental frequencies at $\omega_1 = 1.13$ along with its higher harmonics such as $2\omega_1 = 2.26$, confirming the dynamics are periodic. However, a quenching from $g = 2$ to $g = 0$ generates another frequency at $\omega_2 = 4.09$ along with ω_1, as shown in Fig. 17(b), indicating the quasiperiodic nature of the dynamics of the condensate. The dynamics of the localized states with higher nonlinearity ($g = 3$) exhibits the generation of more frequencies around the two frequencies ω_1 and ω_2, as illustrated in Figs. 17(c) and 17(d). However, for $g \gtrsim 5$, more frequencies start appearing near ω_1 and ω_2 in the PSD. The condensate has a delocalized ground state for $g \gtrsim 5$ and shows the presence of a wide range of frequencies in the dynamics; the corresponding PSD shows the exponential variation with the angular frequency, a typical signature of the chaotic dynamics. The PSD plots for $g = 6$ [Fig. 17(e)] and $g = 10$ [Fig. 17(f)] indeed show the exponential distribution with the frequencies. Interestingly, similar to the case of a quasiperiodic potential, we find that the delocalized state exhibits a chaotic state when the condensate is trapped in a random disordered potential. The quasiperiodic route to the chaos that exists in the dynamics is similar to that obtained with the condensate trapped in the quasiperiodic potential.

As we decrease the strength of the random disordered potential, the critical value of the nonlinearity at which the chaotic behavior appears in the time correlator decreases. Figure 18 depicts $c(t)$ at different nonlinearity for the disorder strength $V_0 = 0.5$ of the random disordered potential. In this case, the nature of $c(t)$ is periodic for $g = 1.4$, quasiperiodic for $g = 2, 3$, and chaotic for $g = 4, 6, 10$. As we analyze the corresponding PSD, we find the presence of a fundamental frequency at $\omega_1 = 0.62$ [as shown in Fig. 19(a)], which is lower than that for $V_0 = 1$, which is $\omega_1 = 1.13$. An increase in $g = 2$ leads to the generation of another frequency $\omega_2 = 1.02$, which is incommensurate with the fundamental frequency ω_1, indicating the quasiperiodic nature of the dynamics [see Fig. 19(b)]. Further, an increase in the nonlinear interaction to $g = 3$ [Fig. 19(c)] and $g = 4$ [Fig. 19(d)] generates other frequencies, whose origin can be understood as a combination of ω_1 and ω_2. However, for $g = 6$ and 10, the PSD exhibits an exponential distribution with the frequencies indicating the fully chaotic state. Interestingly, the route to chaos for $V_0 = 0.5$ remains a quasiperiodic route, similar to what we obtained for $V_0 = 1$. After associating the delocalized state with the chaotic dynamics, we now focus on complementing the studies by computing the maximal Lyapunov exponent $\lambda_{\max}$ of the time series $c(t)$. In Fig. 20 we plot the variation of $\lambda_{\max}$ averaged over five different random realizations with g for different sets of V_0. For a given V_0, $\lambda_{\max}$ remains negative or close to zero for the localized state, while it becomes positive for the delocalized state. For instance, for $V_0 = 1$, $\lambda_{\max} \sim 0$ for $g \lesssim 3.8$. However, beyond this nonlinearity, $\lambda_{\max}$ becomes positive and remains above zero for a higher value of g. The threshold value of the nonlinearity for $V_0 = 1$ indicates the

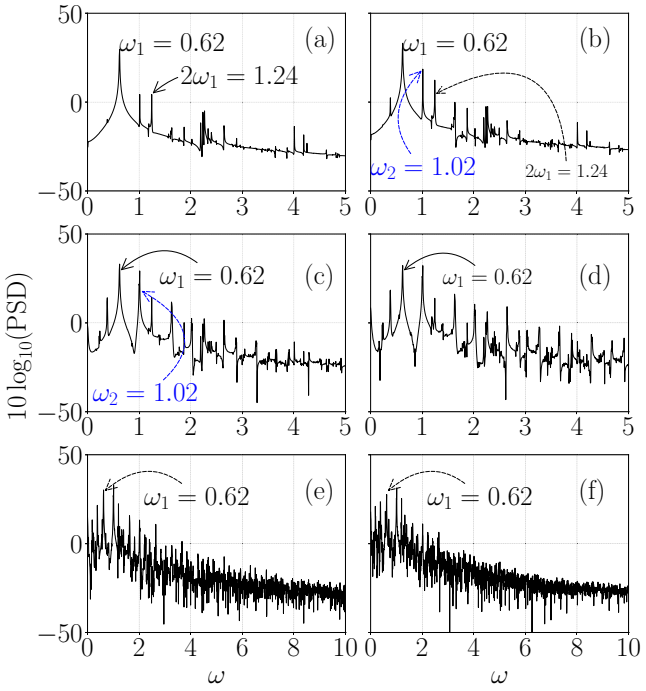

FIG. 19. PSD of the time-correlation function (as shown in Fig. 18) at $V_0 = 0.5$ after quenching at different nonlinearities (a) $g = 1.4$, (b) $g = 2$, (c) $g = 3$, (d) $g = 4$, (e) $g = 6$, and (f) $g = 10$ to $g = 0$. Increasing the nonlinearity generates two incommensurate frequencies $\omega_1 = 0.62$ and $\omega_2 = 1.02$ at $g \sim 2$. Here frequencies get populated near ω_1 and ω_2 when we quench the system from low nonlinearity rather than $V_0 = 1.0$.

delocalized feature of the condensate. Decreasing the potential strength to $V_0 = 0.5$ decreases the threshold nonlinearity to $g_c \sim 2.4$. A further decrease to $V_0 = 0.3$ makes $g_c \sim 2.0$.

In Fig. 21 we present a comparative analysis of the g_c at which the dynamics of the condensate begins to exhibit a positive Lyapunov exponent for both the quasiperiodic optical lattice (blue circles) and the random disordered potential (red diamonds). We observe that the critical value g_c increases for both potentials as the disorder strength increases. Although g_c appears to be of the same order for both disorder potentials at low disorder strengths, for higher disorder strengths g_c is higher for the quasiperiodic potentials than for the random disordered potentials.

V. CONCLUSION

In this paper we have studied the effect of atomic interaction on the ground state and the associated dynamics of Bose-Einstein condensates in a one-dimensional bichromatic optical lattice and random disordered potentials. We identified that increasing the nonlinearity strength leads to the delocalization of the condensates. We analyzed the condensate dynamics by quenching the nonlinearities to zero from the value at which we prepared the ground state. We noticed the regular dynamics of the condensate for small nonlinear strengths, while it became chaotic at large nonlinearities where delocalization occurred. We also identified a quasiperiodic route to chaos for both bichromatic and random

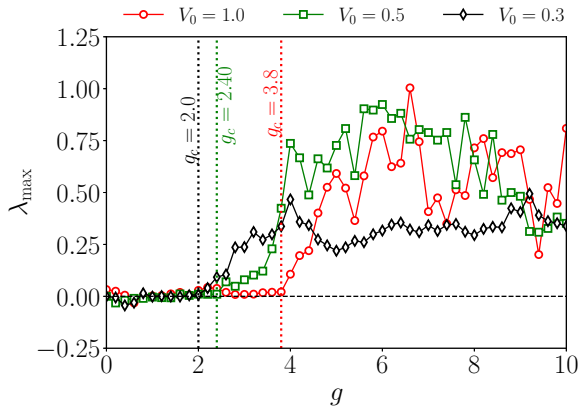

FIG. 20. Maximal Lyapunov exponent $\lambda_{\max}$ averaged over five different random realizations, plotted against nonlinearity for different strengths of the random potential: $V_0 = 1$ (red circles), $V_0 = 0.5$ (green squares), and $V_0 = 0.3$ (black diamonds). The localized state has $\lambda_{\max} \lesssim 0$, while the delocalized states have $\lambda_{\max} > 0$, indicating chaotic dynamics. The threshold g_c above which $\lambda_{\max} > 0$, a characteristic of the delocalized state, decreases as V_0 decreases. Vertical dotted lines are included to guide the eyes for different g_c values. The g_c value is evaluated by taking the average over five realizations.

disordered potentials. The power spectral density displayed a broadband spectrum and the maximal Lyapunov exponent was positive when it exhibited chaotic dynamics. The power spectral density and largest Lyapunov exponent confirmed the presence of chaotic dynamics. Further, we found that the critical nonlinearity for delocalization decreases by decreasing the ratio of amplitudes of the secondary to the primary laser for a quasiperiodic potential or the strength of the random disordered potential. Our study upon quenching the nonlinear interaction revealed the regular dynamics of the condensate for the localized state, while it became chaotic for the delocalized state. In this study, we restricted our analysis to the scalar BECs. However, it would be interesting to extend the work

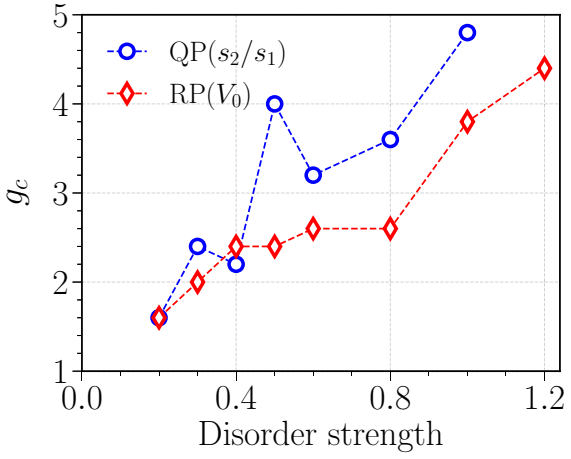

FIG. 21. Variation of the critical nonlinearity strength g_c with the disorder strength ratio s_2/s_1 for the quasiperiodic (QP) lattice and the potential strength V_0 for the random potential (RP). The data points for the random potential are the averaged data over five different disorder realizations.

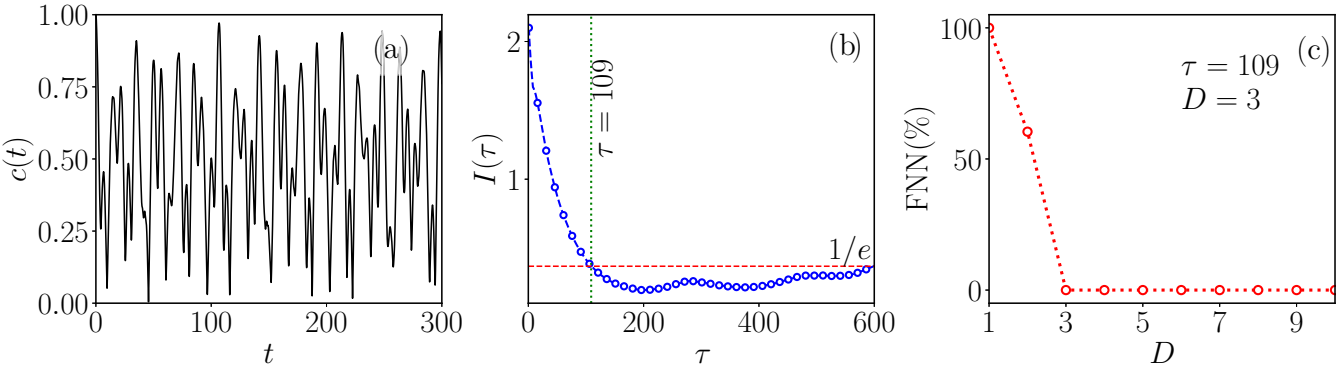

FIG. 22. (a) Temporal variation of the time-correlator function $c(t)$ at $g = 9.0$ and $s_2/s_1 = 1.0$. (b) Variation of the average mutual information with the time delay τ of $c(\tilde{t})$. Here the value of the optimum time delay $\tau = 109$ is estimated using the $1/e$ fall of the AMI function. The red dashed line is drawn at $1/e$ as a guide for estimating the optimum value. (c) Variation of false nearest neighbors with the embedding dimension D. The optimum embedding dimension D turns out to be 3, where the FNN falls to zero.

for the spin-orbit-coupled spinor BECs where the quenching of coupling parameters has an effect similar to quenching of the nonlinear interaction and thus has the possibility of richer dynamics [55]. Also, it would be interesting to extend the work for a finite quenching rate.

ACKNOWLEDGMENTS

We thank Kanhaiya Pandey, Sadhan K. Adhikari, Luca Salasnich, and Saptarishi Chaudhuri for the fruitful discussions and suggestions. We also gratefully acknowledge our supercomputing facility Param-Ishan (IITG), where all the simulation runs were performed. The work of P.M. was supported by DST-SERB under Grant No. CRG/2019/004059, DST-FIST under Grant No. SR/FST/PSI-204/2015(C), and MoE RUSA 2.0 (Physical Sciences). P.K.M. acknowledges the Department of Science and Technology–Science and Engineering Research Board India for financial support through Project No. ECR/2017/002639.

APPENDIX: SELECTION CRITERIA FOR THE EMBEDDING DIMENSION AND DELAY TIME OF TIME SERIES OF THE CORRELATION FUNCTION

In this Appendix we provide details on the steps involved in choosing a proper embedding dimension and delay time to obtain the maximal Lyapunov exponent $\lambda_{\max}$ from the time series of the correlation function. The first step involves reconstructing the phase space from the time series data. Let us assume we have a set of N discrete data points in the time series of the correlation function, given as $c_1, c_2, c_3, c_4, \ldots, c_N$. By considering the delay time τ and an embedding dimension D, we obtain the D-dimensional delay coordinate as $Y(\tilde{t}) = (c(\tilde{t}), c(\tilde{t}+\tau), \ldots, c(\tilde{t}+(D-1)\tau))$. Note that both $\tilde{t} \in [1, N]$ and $\tau \in [1, N]$ are integers used to index the time series data of $c(t)$, which can be mapped to the real time by multiplying by the factor dt. Usually, the choice of τ is such that the values of $c(\tilde{t})$ and $c(\tilde{t}+\tau)$ are sufficiently independent to be useful components of the time-correlator vector $c(\tilde{t})$, but they should not be so independent that they have no connection at all. To choose the optimum value of τ, we calculate the average mutual information $I(\tau)$ of the variable $c(\tilde{t})$ and $c(\tilde{t}+\tau)$ for various values of τ given as [80]

$$I(\tau) = \sum_i \sum_j P_{i,j}(\tau) \log_2 \frac{P_{i,j}(\tau)}{P_i P_j}. \tag{A1}$$

Here P_i represents the probability that $c(\tilde{t})$ falls inside the ith bin of the histogram constructed from the data points of c and $P_{i,j}$ is the joint probability that $c(\tilde{t})$ and $c(\tilde{t}+\tau)$ should come under the ith and jth bins of the histogram, respectively. Following this, the optimum τ is calculated by examining the value of τ at which $I(\tau)$ either achieves its first minimum [80] or drops below the value of $1/e$ [81]. Whichever criterion gives the minimum τ is chosen. This value of τ represents the delay time at which $c(\tilde{t}+\tau)$ contributes the maximum information to our knowledge of $c(\tilde{t})$. The next step is to determine the embedding dimension D, which can be estimated using the method of false nearest neighbors. In this process, we consider the data points that are neighbors to each other in the original one-dimensional time series of $c(\tilde{t})$. Then we check the separation between these neighbors when the time series is embedded in a higher-dimensional space. If the embedding process significantly changes the distance between the neighboring points, they are referred to as false neighbors, indicating the need to increase D. Therefore, the entire scheme is based on gradually increasing the embedding dimension D for the optimum τ and computing the percentage of false neighbors with respect to the true neighbors for each value of D. Only the value of D for which the number of FNNs drops to 0 or subsequent increments in D leave the FNNs unchanged is considered the optimum embedding dimension. Let us denote the ith nearest neighbor of the coordinate vector $Y(\tilde{t})$ by $Y^i(\tilde{t})$. The separation between them can be represented in the D-dimensional phase space as

$$R_D^2(\tilde{t}, i) = \sum_{j=0}^{D-1} [c(\tilde{t}+j\tau) - c^{(i)}(\tilde{t}+j\tau)]^2. \tag{A2}$$

Following the above discussion, as we go from a D-dimensional phase space to a $(D+1)$-dimensional phase space using time-delayed embedding, the separation between

the ith neighbors of a new vector $Y(\tilde{t})$ can be written as

$$R^2_{D+1}(\tilde{t}, i) = R^2_D(\tilde{t}, i) + [c(\tilde{t} + D\tau) - c^{(i)}(\tilde{t} + D\tau)]^2. \quad \text{(A3)}$$

In Fig. 22 we demonstrate the calculation of τ and D using the chaotic time series of the time correlator obtained after the quenching of the ground state prepared for $g = 9.0$ and $s_2/s_1 = 1.0$, with other parameters the same as those in Fig. 1. Following the method discussed above, we obtain the optimum τ and D as 109 and 3, respectively, for this case.

[1] G. Modugno, Anderson localization in Bose-Einstein condensates, Rep. Prog. Phys. **73**, 102401 (2010).

[2] A. Lagendijk, B. van Tiggelen, and D. S. Wiersma, Fifty years of Anderson localization, Phys. Today **62**(8), 24 (2009).

[3] A. Aspect and M. Inguscio, Anderson localization of ultracold atoms, Phys. Today **62**(8), 30 (2009).

[4] P. W. Anderson, Absence of diffusion in certain random lattices, Phys. Rev. **109**, 1492 (1958).

[5] D. S. Wiersma, P. Bartolini, A. Lagendijk, and R. Righini, Localization of light in a disordered medium, Nature (London) **390**, 671 (1997).

[6] F. Scheffold, R. Lenke, R. Tweer, and G. Maret, Localization or classical diffusion of light? Nature (London) **398**, 206 (1999).

[7] T. Schwartz, G. Bartal, S. Fishman, and M. Segev, Transport and anderson localization in disordered two-dimensional photonic lattices, Nature (London) **446**, 52 (2007).

[8] C. M. Aegerter, M. Störzer, S. Fiebig, W. Bührer, and G. Maret, Observation of Anderson localization of light in three dimensions, J. Opt. Soc. Am. A **24**, A23 (2007).

[9] J. Topolancik, B. Ilic, and F. Vollmer, Experimental Observation of Strong Photon Localization in Disordered Photonic Crystal Waveguides, Phys. Rev. Lett. **99**, 253901 (2007).

[10] R. Dalichaouch, J. P. Armstrong, S. Schultz, P. M. Platzman, and S. L. McCall, Microwave localization by two-dimensional random scattering, Nature (London) **354**, 53 (1991).

[11] C. Dembowski, H.-D. Gräf, R. Hofferbert, H. Rehfeld, A. Richter, and T. Weiland, Anderson localization in a string of microwave cavities, Phys. Rev. E **60**, 3942 (1999).

[12] A. A. Chabanov, M. Stoytchev, and A. Z. Genack, Statistical signatures of photon localization, Nature (London) **404**, 850 (2000).

[13] P. Pradhan and S. Sridhar, Correlations due to Localization in Quantum Eigenfunctions of Disordered Microwave Cavities, Phys. Rev. Lett. **85**, 2360 (2000).

[14] R. Weaver, Anderson localization of ultrasound, Wave Motion **12**, 129 (1990).

[15] H. Hu, A. Strybulevych, J. Page, S. E. Skipetrov, and B. A. van Tiggelen, Localization of ultrasound in a three-dimensional elastic network, Nat. Phys. **4**, 945 (2008).

[16] M. E. Manley, J. W. Lynn, D. Abernathy, E. Specht, O. Delaire, A. Bishop, R. Sahul, and J. Budai, Phonon localization drives polar nanoregions in a relaxor ferroelectric, Nat. Commun. **5**, 3683 (2014).

[17] F. L. Moore, J. C. Robinson, C. Bharucha, P. E. Williams, and M. G. Raizen, Observation of Dynamical Localization in Atomic Momentum Transfer: A New Testing Ground for Quantum Chaos, Phys. Rev. Lett. **73**, 2974 (1994).

[18] J. Chabé, G. Lemarié, B. Grémaud, D. Delande, P. Szriftgiser, and J. C. Garreau, Experimental Observation of the Anderson Metal-Insulator Transition with Atomic Matter Waves, Phys. Rev. Lett. **101**, 255702 (2008).

[19] J. Billy, V. Josse, Z. Zuo, A. Bernard, B. Hambrecht, P. Lugan, D. Clément, L. Sanchez-Palencia, P. Bouyer, and A. Aspect, Direct observation of anderson localization of matter waves in a controlled disorder, Nature (London) **453**, 891 (2008).

[20] G. Roati, C. D'Errico, L. Fallani, M. Fattori, C. Fort, M. Zaccanti, G. Modugno, M. Modugno, and M. Inguscio, Anderson localization of a non-interacting Bose-Einstein condensate, Nature (London) **453**, 895 (2008).

[21] D. H. White, T. A. Haase, D. J. Brown, M. D. Hoogerland, M. S. Najafabadi, J. L. Helm, C. Gies, D. Schumayer, and D. A. W. Hutchinson, Observation of two-dimensional Anderson localisation of ultracold atoms, Nat. Commun. **11**, 4942 (2020).

[22] S. E. Skipetrov, A. Minguzzi, B. A. van Tiggelen, and B. Shapiro, Anderson Localization of a Bose-Einstein Condensate in a 3D Random Potential, Phys. Rev. Lett. **100**, 165301 (2008).

[23] S. K. Adhikari and L. Salasnich, Localization of a Bose-Einstein condensate in a bichromatic optical lattice, Phys. Rev. A **80**, 023606 (2009).

[24] P. Muruganandam, R. K. Kumar, and S. K. Adhikari, Localization of a dipolar Bose-Einstein condensate in a bichromatic optical lattice, J. Phys. B **43**, 205305 (2010).

[25] Y. Cheng and S. K. Adhikari, Symmetry breaking in a localized interacting binary Bose-Einstein condensate in a bichromatic optical lattice, Phys. Rev. A **81**, 023620 (2010).

[26] Y. Cheng and S. Adhikari, Spatially-antisymmetric localization of matter wave in a bichromatic optical lattice, Laser Phys. Lett. **7**, 824 (2010).

[27] Y. Cheng and S. K. Adhikari, Localization of a Bose-Fermi mixture in a bichromatic optical lattice, Phys. Rev. A **84**, 023632 (2011).

[28] Y. Cheng and S. K. Adhikari, Matter-wave localization in a weakly perturbed optical lattice, Phys. Rev. A **84**, 053634 (2011).

[29] Y. Cheng, G. Tang, and S. K. Adhikari, Localization of a spin-orbit-coupled Bose-Einstein condensate in a bichromatic optical lattice, Phys. Rev. A **89**, 063602 (2014).

[30] C. Li, F. Ye, Y. V. Kartashov, V. V. Konotop, and X. Chen, Localization-delocalization transition in spin-orbit-coupled Bose-Einstein condensate, Sci. Rep. **6**, 31700 (2016).

[31] D. M. Abrams, R. Mirollo, S. H. Strogatz, and D. A. Wiley, Solvable Model for Chimera States of Coupled Oscillators, Phys. Rev. Lett. **101**, 084103 (2008).

[32] B. Deissler, M. Zaccanti, G. Roati, C. D'Errico, M. Fattori, M. Modugno, G. Modugno, and M. Inguscio, Delocalization of a disordered bosonic system by repulsive interactions, Nat. Phys. **6**, 354 (2010).

[33] Y. Cheng and S. K. Adhikari, Matter-wave localization in a random potential, Phys. Rev. A **82**, 013631 (2010).

[34] W. Cardoso, A. Avelar, and D. Bazeia, Anderson localization of matter waves in chaotic potentials, Nonlinear Anal. Real World Appl. **13**, 755 (2012).

[35] K.-T. Xi, J. Li, and D.-N. Shi, Localization of a two-component Bose-Einstein condensate in a one-dimensional random potential, Physica B **459**, 6 (2015).

[36] H. Zhang, S. Liu, and Y. Zhang, Anderson localization of a spin-orbit coupled Bose-Einstein condensate in disorder potential, Chin. Phys. B **31**, 070305 (2022).

[37] A. S. Pikovsky and D. L. Shepelyansky, Destruction of Anderson Localization by a Weak Nonlinearity, Phys. Rev. Lett. **100**, 094101 (2008).

[38] E. Lucioni, B. Deissler, L. Tanzi, G. Roati, M. Zaccanti, M. Modugno, M. Larcher, F. Dalfovo, M. Inguscio, and G. Modugno, Observation of Subdiffusion in a Disordered Interacting System, Phys. Rev. Lett. **106**, 230403 (2011).

[39] G. Kopidakis, S. Komineas, S. Flach, and S. Aubry, Absence of Wave Packet Diffusion in Disordered Nonlinear Systems, Phys. Rev. Lett. **100**, 084103 (2008).

[40] N. Cherroret, B. Vermersch, J. C. Garreau, and D. Delande, How Nonlinear Interactions Challenge the Three-Dimensional Anderson Transition, Phys. Rev. Lett. **112**, 170603 (2014).

[41] E. V. H. Doggen and J. J. Kinnunen, Quench-induced delocalization, New J. Phys. **16**, 113051 (2014).

[42] R. C. Kuhn, C. Miniatura, D. Delande, O. Sigwarth, and C. A. Müller, Localization of Matter Waves in Two-Dimensional Disordered Optical Potentials, Phys. Rev. Lett. **95**, 250403 (2005).

[43] B. Damski, J. Zakrzewski, L. Santos, P. Zoller, and M. Lewenstein, Atomic Bose and Anderson Glasses in Optical Lattices, Phys. Rev. Lett. **91**, 080403 (2003).

[44] L. Sanchez-Palencia, D. Clément, P. Lugan, P. Bouyer, G. V. Shlyapnikov, and A. Aspect, Anderson Localization of Expanding Bose-Einstein Condensates in Random Potentials, Phys. Rev. Lett. **98**, 210401 (2007).

[45] P. Lugan, D. Clément, P. Bouyer, A. Aspect, and L. Sanchez-Palencia, Anderson Localization of Bogolyubov Quasiparticles in Interacting Bose-Einstein Condensates, Phys. Rev. Lett. **99**, 180402 (2007).

[46] S. Mardonov, M. Modugno, and E. Y. Sherman, Dynamics of Spin-Orbit Coupled Bose-Einstein Condensates in a Random Potential, Phys. Rev. Lett. **115**, 180402 (2015).

[47] S. Mardonov, V. V. Konotop, B. A. Malomed, M. Modugno, and E. Y. Sherman, Spin-orbit-coupled soliton in a random potential, Phys. Rev. A **98**, 023604 (2018).

[48] S. Mardonov, M. Modugno, E. Y. Sherman, and B. A. Malomed, Rabi-coupling-driven motion of a soliton in a Bose-Einstein condensate, Phys. Rev. A **99**, 013611 (2019).

[49] I. Březinová, L. A. Collins, K. Ludwig, B. I. Schneider, and J. Burgdörfer, Wave chaos in the nonequilibrium dynamics of the Gross-Pitaevskii equation, Phys. Rev. A **83**, 043611 (2011).

[50] P. Muruganandam and S. K. Adhikari, Chaotic oscillation in an attractive Bose-Einstein condensate under an impulsive force, Phys. Rev. A **65**, 043608 (2002).

[51] P. Verma, A. Bhattacherjee, and M. Mohan, Chaos in BEC trapped in tilted optical superlattice potential with attractive interaction, J. Phys.: Conf. Ser. **350**, 012003 (2012).

[52] E. Tosyali, F. Aydogmus, and A. Yilmaz, Regular and chaotic solutions in BEC for tilted bichromatical optical lattice, Int. J. Mod. Phys. B **32**, 1850254 (2018).

[53] N. Cherroret, T. Scoquart, and D. Delande, in *Special Issue on Localisation 2020*, edited by S. Kettemann and R. Bhatt, Coherent multiple scattering of out-of-equilibrium interacting Bose gases, Ann. Phys. (NY) **435**, 168543 (2021).

[54] R. Ravisankar, T. Sriraman, L. Salasnich, and P. Muruganandam, Quenching dynamics of the bright solitons and other localized states in spin–orbit coupled Bose-Einstein condensates, J. Phys. B **53**, 195301 (2020).

[55] S. Gangwar, R. Ravisankar, P. Muruganandam, and P. K. Mishra, Dynamics of quantum solitons in Lee-Huang-Yang spin-orbit-coupled Bose-Einstein condensates, Phys. Rev. A **106**, 063315 (2022).

[56] R. Du, J.-C. Xing, B. Xiong, J.-H. Zheng, and T. Yang, Quench dynamics of Bose-Einstein condensates in boxlike traps, Chin. Phys. Lett. **39**, 070304 (2022).

[57] L. Sanchez-Palencia, D. Clément, P. Lugan, P. Bouyer, and A. Aspect, Disorder-induced trapping versus Anderson localization in Bose-Einstein condensates expanding in disordered potentials, New J. Phys. **10**, 045019 (2008).

[58] L. Sanchez-Palencia and M. Lewenstein, Disordered quantum gases under control, Nat. Phys. **6**, 87 (2010).

[59] Y. Shin, M. Saba, T. A. Pasquini, W. Ketterle, D. E. Pritchard, and A. E. Leanhardt, Atom Interferometry with Bose-Einstein Condensates in a Double-Well Potential, Phys. Rev. Lett. **92**, 050405 (2004).

[60] M. Saba, T. Pasquini, C. Sanner, Y. Shin, W. Ketterle, and D. Pritchard, Light scattering to determine the relative phase of two Bose-Einstein condensates, Science **307**, 1945 (2005).

[61] Y. Shin, G.-B. Jo, M. Saba, T. A. Pasquini, W. Ketterle, and D. E. Pritchard, Optical Weak Link between Two Spatially Separated Bose-Einstein Condensates, Phys. Rev. Lett. **95**, 170402 (2005).

[62] C. Chin, R. Grimm, P. Julienne, and E. Tiesinga, Feshbach resonances in ultracold gases, Rev. Mod. Phys. **82**, 1225 (2010).

[63] H. Ott, J. Fortágh, S. Kraft, A. Günther, D. Komma, and C. Zimmermann, Nonlinear Dynamics of a Bose-Einstein Condensate in a Magnetic Waveguide, Phys. Rev. Lett. **91**, 040402 (2003).

[64] K. D. Rao and M. Swamy, *Digital Signal Processing: Theory and Practice* (Springer, Singapore, 2018), pp. 721–751.

[65] S. Dalui, B. R. Majhi, and P. Mishra, Induction of chaotic fluctuations in particle dynamics in a uniformly accelerated frame, Int. J. Mod. Phys. A **35**, 2050081 (2020).

[66] I. Vlachos and D. Kugiumtzis, in *Topics on Chaotic Systems*, edited by C. H. Skiadas, I. Dimotikalis, and C. Skiadas (World Scientific, Singapore, 2009), pp. 378–387.

[67] M. B. Kennel, R. Brown, and H. D. I. Abarbanel, Determining embedding dimension for phase-space reconstruction using a geometrical construction, Phys. Rev. A **45**, 3403 (1992).

[68] S. Wallot and D. Mønster, Calculation of average mutual information (AMI) and false-nearest neighbors (FNN) for the estimation of embedding parameters of multidimensional time series in matlab, Front. Psychol. **9**, 1679 (2018).

[69] A. Wolf, J. B. Swift, H. L. Swinney, and J. A. Vastano, Determining Lyapunov exponents from a time series, Physica D **16**, 285 (1985).

[70] P. Muruganandam and S. Adhikari, Fortran programs for the time-dependent Gross-Pitaevskii equation in a fully anisotropic trap, Comput. Phys. Commun. **180**, 1888 (2009).

[71] L. E. Young-S., P. Muruganandam, S. K. Adhikari, V. Lončar, D. Vudragović, and A. Balaž, OpenMP GNU and Intel Fortran programs for solving the time-dependent Gross-Pitaevskii equation, Comput. Phys. Commun. **220**, 503 (2017).

[72] D. E. Sigeti, Exponential decay of power spectra at high frequency and positive Lyapunov exponents, Physica D **82**, 136 (1995).

[73] U. Frisch and R. Morf, Intermittency in nonlinear dynamics and singularities at complex times, Phys. Rev. A **23**, 2673 (1981).

[74] I. M. Lifshits, S. A. Gredeskul, and L. A. Pastur, *Introduction to the Theory of Disordered Systems* (Wiley-VCH, Weinheim, 1988).

[75] M. P. A. Fisher, P. B. Weichman, G. Grinstein, and D. S. Fisher, Boson localization and the superfluid-insulator transition, Phys. Rev. B **40**, 546 (1989).

[76] R. T. Scalettar, G. G. Batrouni, and G. T. Zimanyi, Localization in Interacting, Disordered, Bose Systems, Phys. Rev. Lett. **66**, 3144 (1991).

[77] F. Stellin, M. Filoche, and F. Dias, Localization landscape for interacting Bose gases in one-dimensional speckle potentials, Phys. Rev. A **107**, 043306 (2023).

[78] P. Lugan, D. Clément, P. Bouyer, A. Aspect, M. Lewenstein, and L. Sanchez-Palencia, Ultracold Bose Gases in 1D Disorder: From Lifshits Glass to Bose-Einstein Condensate, Phys. Rev. Lett. **98**, 170403 (2007).

[79] M. C. P. dos Santos and W. B. Cardoso, Anderson localization induced by interaction in linearly coupled binary Bose-Einstein condensates, Phys. Rev. E **103**, 052210 (2021).

[80] A. M. Fraser and H. L. Swinney, Independent coordinates for strange attractors from mutual information, Phys. Rev. A **33**, 1134 (1986).

[81] H. Kantz and T. Schreiber, *Nonlinear Time Series Analysis* (Cambridge University Press, Cambridge, 2004), Vol. 7.